ADVANCED NANOBIOMED RESEARCH
www.advnanobiomedres.com

Biomedical Applications of Magnetic Levitation

Sajjad Rahmani Dabbagh, M. Munzer Alseed, Milad Saadat, Metin Sitti, and SavasTasoglu**

Magnetic levitation (MagLev) is a user-friendly, electricity-free, accurate, affordable, and label-free platform for chemical and biological applications owing to its ability to suspend and separate a wide range of diamagnetic materials (e.g., plastics, polymers, cells, and proteins) based on their density. Various MagLev designs (e.g., standard, single and double ring, titled, and rotational MagLev setups) are presented in the literature with a trade-off between sensitivity and detection range. Herein, various MagLev designs, the advantages and pitfalls of each method, and current challenges encountered by MagLev platforms are reviewed. Moreover, end applications of MagLev are presented in single-cell and protein analysis, diseases diagnosis (e.g., cancer and hepatitis C), tissue engineering, 3D self-assembly, and forensic case studies to provide an insight regarding the potentials of MagLev.

1. Introduction

Volumetric mass density can be used to analyze and track various biological and chemical states and processes, including chemical reactions, quality of micro/milli-plastic products, degree of polymerization, protein binding, and cell pathophysiology as well as cellular physiological changes, because the density of cells changes during a number of processes such as malignant transformation.[1–5] Density-based particle separation methods rely solely on "density" while substantially insensitive to mechanical properties of matter (e.g., shape, size, viscosity, elasticity, and tensile strength), enabling the density measurement of irregular-shaped materials.[1,6]

Several techniques are at a researcher's disposal when wishing to measure density. Hydrometers and pycnometers both work based on the displaced fluid principle and are inexpensive devices. However, they are limited to liquid samples, a large sample volume is needed, readings for such devices are time-consuming[7] and may come with errors due to the presence of solids and gases, and also the temperature control is necessary for precise density measurement.[8] On the other hand, helium pycnometers and density gradient columns are limited to solid samples and are not portable.[9] Besides, hydrostatic balances are expensive and very time-consuming. Another disadvantage is that installation (e.g., insulation on a concrete foundation) is challenging, and accurate temperature control is essential. Microchannel resonators are other options to quantify the density through the change in resonance frequency from the baseline as the sample passes a cantilever channel. Such devices have high pressure sensitivity and channel resistance, compromising their overall throughput.[10] Dielectrophoretic (DEP) flow-field fractionation is a biocompatible technique that exploits the balance of DEP levitation and gravitation forces.[11] DEP devices have the drawback of low throughput, Joule heating, complex design criteria, and the requirement of pretreatment steps.[12]

On the other hand, magnetic levitation (MagLev) opens a unique paradigm for density-based separation, analysis, and 3D self-assembly based on the equilibrium between the magnetic, buoyant, and gravitational forces.[13,14] MagLev was traditionally used for vehicle[15] and train[16–18] suspension. Moreover, by using an electromagnetic field, MagLev found an application in the levitation of strongly diamagnetic materials (e.g., pyrolytic graphite and bismuth) in the air (1939).[19] Subsequently, MagLev was used in the fabrication of frictionless rotors (1966),[20] tiltmeter (1968),[21] and accelerometers (1969),[22] followed by the separation of plastic, metals, and minerals (1976).[23] As a result of using resistive solenoid electromagnets and superconductors, in the 1990s, living organisms,

S. R. Dabbagh, M. Saadat, M. Sitti, S. Tasoglu
Department of Mechanical Engineering
Koç University
Sariyer, Istanbul, Turkey 34450
E-mail: sitti@is.mpg.de; stasoglu@ku.edu.tr

S. R. Dabbagh, S. Tasoglu
Koç University Arçelik Research Center for Creative Industries (KUAR)
Koç University
Sariyer, Istanbul, Turkey 34450

M. M. Alseed, S. Tasoglu
Institute of Biomedical Engineering
Boğaziçi University
Çengelköy, Istanbul, Turkey 34684

M. Sitti
School of Medicine
Koç University
Istanbul 34450, Turkey

M. Sitti, S. Tasoglu
Physical Intelligence Department
Max Planck Institute for Intelligent Systems
70569 Stuttgart, Germany

The ORCID identification number(s) for the author(s) of this article can be found under https://doi.org/10.1002/anbr.202100103.

© 2021 The Authors. Advanced NanoBiomed Research published by Wiley-VCH GmbH. This is an open access article under the terms of the Creative Commons Attribution License, which permits use, distribution and reproduction in any medium, provided the original work is properly cited.

DOI: 10.1002/anbr.202100103

ethanol, water, wood, and glass were levitated by MagLev.[1,24–26] The advancement in Neodymium (NdFeB) magnets (1984) contributed significantly to the expansion of electricity-free, portable MagLev platforms in density measurement.[1,27,28] The potency of MagLev techniques has led to the introduction of this method into heart valves,[29] fans,[30] and density measurement in recent years.[31–34]

MagLev devices are portable,[35] low cost,[36,37] label-free,[38–41] easy to use,[42] and accurate.[9,43] MagLev has applications in measuring the density of polymers and characterizing polymer composition,[4,9] and analysis of crystal polymorphs,[3] biopolymers,[9] chemicals, biochemical particles,[1] nutrition content of food products (e.g., dairy),[44] and proteins.[37,45–48] In the specific context of biological assay, MagLev demonstrated excellent potential for cell analysis,[49,50] quantification of protein binding degree[5] and measurement of antigen–antibodies binding in quantitative immunoassays,[51] disease diagnosis[38,52] (e.g., cancer cells,[40,53–56] sepsis,[57] and hepatitis C[58]), and blood analysis.[59] Moreover, MagLev is actively playing a role in the density measurement of illicit drugs and powders, as well as forensic samples,[14,60,61] 3D cell culturing,[62,63] and tissue engineering.[64–67] More recently, MagLev platforms have been integrated with smartphones[38,41,59] and fluorescent imaging[35] to further promote their versatility and portability in resource-limited settings.

In this review article, the working principles of MagLev devices are described, and the decisive design parameters of MagLev platforms are introduced. Additionally, we review the state-of-the-art MagLev designs and end applications spanning over disease diagnosis (cancer detection, blood analysis, and protein analysis), biological assay (forensic evaluation, single-cell analysis, bone analysis, cell sorting, and identification), and tissue engineering (3D cell culturing and scaffold-free biofabrication). Finally, current challenges (and recommendations for overcoming them) of developing MagLev platforms for future studies are provided.

2. Magnetic Levitation Fundamentals

The word "magnet" has a Greek root "magnēs lithos,"[68] meaning "the Magnesian stone, lodestone."[69] Magnetic materials are traditionally classified based on their bulk susceptibility (χ),[70] i.e., the ratio of magnetization upon the magnetic field strength ($\chi = M/H$).[71] Diamagnetic materials oppose the applied magnetic field, attaining a negative magnetic susceptibility (-10^{-5}).[72] The second type of magnetic materials—paramagnetic materials—has small χ (around 10^{-5} to 10^{-3}) and is weakly attracted in a magnetic field. The other group of magnetism is called ferromagnetism. Ferromagnetic materials have a magnetic susceptibility much higher than unity.[70] When the size of ferromagnetic materials reduces to a critical value (e.g., 10–20 nm in diameter for iron oxides[73]), these materials become single domain,[74] therefore responding faster and stronger to applied magnetic fields[73] without any magnetic memory.[75] Most materials are diamagnetic, including graphite, water, most polymers, colloidal suspensions, heterogeneous materials, pastes, gels, liquids, and organic matter—all organic matter is diamagnetic, except stable free radicals.[6,9] There are also other categories of magnetic materials outside the scope of this review article.[70,72]

Attracted materials to a magnet have unpaired electrons in their outer shell. When exposed to a magnet, these unpaired electrons create a small magnetic field that may aggregate to create a strong magnetic field around the material.[76] As magnetism is the inherent property of matter, the susceptibility difference induces a magnetic force under an external magnetic field, meaning that magnetic manipulation of microparticles or cells is possible. Therefore, target objects (e.g., cells or particles) can be separated from heterogeneous mixtures under a magnetic field.[77] Being inexpensive and easy to use,[77] magnetic field-based manipulation methods have shown to be promising for the small-scale motion control of objects.[78] These manipulations have applications in magnetic separation,[79–82] droplet manipulation,[83–85] focusing and sorting,[86,87] detection,[88,89] and mixing.[90–93]

The magnetic susceptibility difference between the object and the medium, under a magnetic field, is exploited to suspend particles,[37] which is either based on positive or negative magnetophoresis. In positive magnetophoresis, paramagnetic materials are manipulated in a diamagnetic medium. However, negative magnetophoresis[94] is a low-cost and convenient method[60] for stably suspending diamagnetic (or weakly paramagnetic) samples in a paramagnetic medium under a magnetic field, which imposes a magnetic force on the diamagnetic sample (e.g., cancer cells, illicit powders, or microparticles) in the field.[94] The term "levitation" is mainly used due to the movements of particles from the walls (where the magnets are often located) toward the channel centroids, in other words from high magnetic field strengths to low magnetic field strengths (i.e., diamagnetic materials in a paramagnetic medium). Therefore, the "MagLev" term is usually dedicated for "negative magnetophoresis," unless otherwise mentioned. This review article focuses on negative magnetophoresis devices (i.e., MagLev devices) and their applications in sample analysis and, specifically, biological sample characterization and measurement.

3. Magnetic Levitation Platforms: Design Perspective

The terms "sensitivity" (i.e., the ability of MagLev to distinguish subtle density differences in levitated objects) and "dynamic range" (i.e., the range of different densities that can be measured) are two important parameters to determine the performance of a MagLev platform. Based on the specific demand, different MagLev platforms are developed to tune the sensitivity and/or the range. In "standard" MagLev, two permanent magnets are placed vertically with like-poles facing.[40,95] In other configurations, axial MagLev devices were developed with either two-ring[34,96–98] or single-ring[99] magnets to improve sensitivity. Stacked,[100] lensless,[50] tilted,[101] horizontal,[66,102] and rotational[103] MagLev devices have also been developed (**Figure 1**).

One major drawback of MagLev platforms is their limited capacity to analyze multiple samples at the same time. When sample analysis time is of importance (e.g., testing several suspicious powder samples simultaneously at airports or police stations), high-throughput configurations with the aid of stacked magnets can be useful to reduce analysis duration. Figure 1A represents a 96-well plate design with stacked magnets which

© 2021 The Authors. Advanced NanoBiomed Research published by Wiley-VCH GmbH

26999307, 2022, 3, Downloaded from https://advanced.onlinelibrary.wiley.com/doi/10.1002/anbr.202100103 by Koc University, Wiley Online Library on [05/09/2026]. See the Terms and Conditions (https://onlinelibrary.wiley.com/terms-and-conditions) on Wiley Online Library for rules of use; OA articles are governed by the applicable Creative Commons License

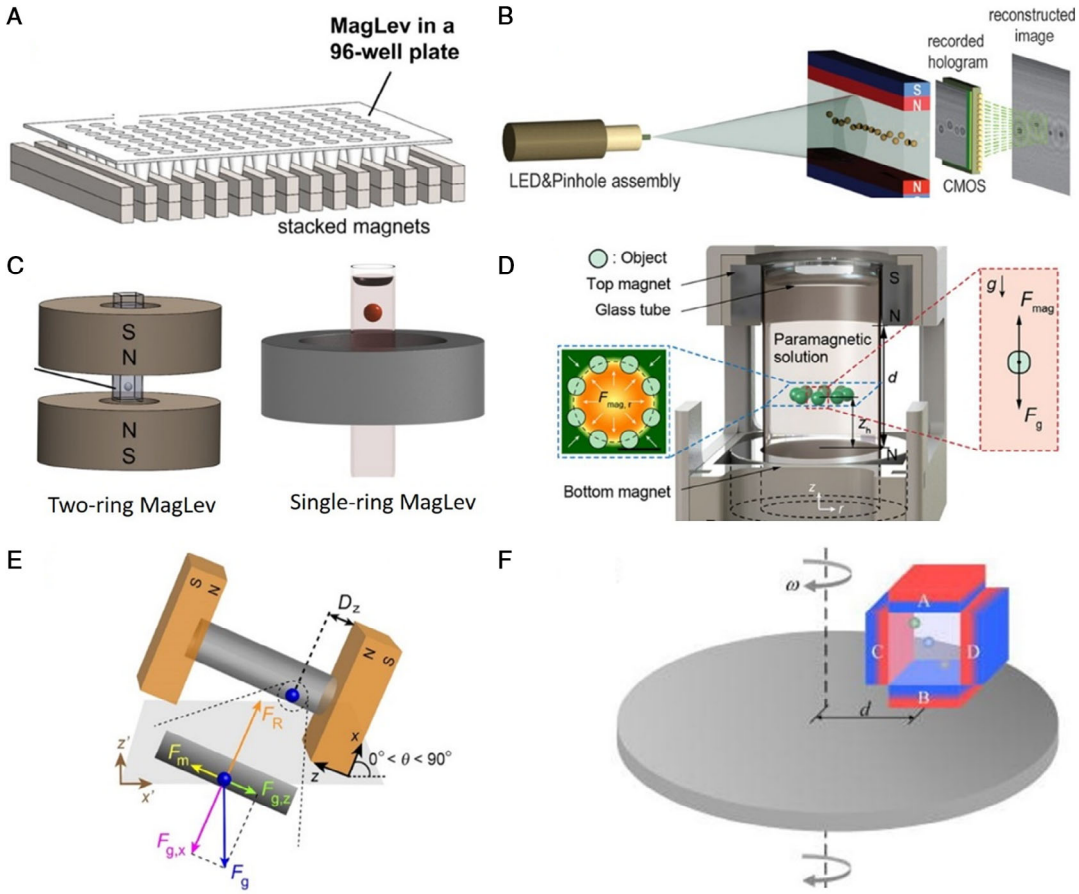


Figure 1. Different MagLev designs. A) The high-throughput design with a 96-well plate and 11 pairs of stacked magnets.[100] Reproduced with permission.[100] Copyright 2018, American Chemical Society. B) Illustration of the lensless MagLev design.[50] Reproduced with permission.[50] Copyright 2021, American Chemical Society. C) (left) The two-ring axial MagLev design[34] and (right) single-ring MagLev.[99] Reproduced with permission.[34,99] Copyright 2018, American Chemical Society. D) The axial-circular MagLev design to perform 3D density measurement.[98] Reproduced with permission.[98] Copyright 2020, American Chemical Society. E) Tilted MagLev device to measure a wider range of densities.[101] Reproduced with permission.[101] Copyright 2016, American Chemical Society. F) Rotational MagLev design.[103] Reproduced with permission.[103] Copyright 2018, AIP Publishing.

enables high throughput analysis of nonmixable samples simultaneously.[100]

To alleviate the issue of bulky and expensive optical instruments in MagLev setups, it is possible to use lensless digital inline holographic microscopy (LDIHM). This design relies on the interference pattern between the light diffracted from samples (e.g., cells) within a microcapillary channel and the undistorted background illumination using a complementary metal–oxide–semiconductor (CMOS) imaging sensor (Figure 1B). The spatial resolution, in this method, is limited to the maximum pixel size of the imaging sensor (e.g., 1.12 μm). The integrated setup (MagLev + LDIHM) cost was less than $100 with a compact size that can fit into a pocket. A challenging task in this method is the thresholding because reconstructed holographic images generate an optical artifact presented in LDIHM accompanying severe irregular background noise.[50]

In contrast to standard MagLev platforms, in which physical barriers may complicate samples or paramagnetic medium addition/withdrawal, in axial MagLev systems with two-ring magnets, these limitations can be partially addressed (Figure 1C). In axial MagLev configurations, as the top end of the container is accessible, it is possible to add or retrieve samples during analysis and also to perform ultrasonic levitation height measurement.[34] Moreover, a 360° view of the sample is available, which allows great control over height recording and density measurement. In addition, this type of MagLev is compatible with different container shapes and sizes. Compared to single-ring magnets, two-magnet systems have several advantages, such as the linear magnetic field (compared with nonlinear magnetic fields generated by single-magnet platforms), which promotes straightforward density measurement, particle alignment along the centerline of magnets, and operational simplicity in density measurement (Figure 1C).[99] On the other hand, two-ring systems have the drawback of short working distance (≈15 mm compared to 45 mm in the standard MagLev device), while this value for nonlinear magnetic fields can be extended at least to ≈38 mm. For single-ring MagLev devices, density measurements as accurate as ±0.0005 to ±0.0078 g cm^{-3} are reported.[99] Besides, two-ring MagLev configurations can be modified for 3D density profile measurement (Figure 1D). In this method, levitation height, in the axial direction, and the circular position of samples were used to perform density measurement. Circular

© 2021 The Authors. Advanced NanoBiomed Research published by Wiley-VCH GmbH

26999307, 2022, 3, Downloaded from https://advanced.onlinelibrary.wiley.com/doi/10.1002/anbr.202100103 by Koc University, Wiley Online Library on [05/09/2026]. See the Terms and Conditions (https://onlinelibrary.wiley.com/terms-and-conditions) on Wiley Online Library for rules of use; OA articles are governed by the applicable Creative Commons License

26999307, 2022, 3, Downloaded from https://advanced.onlinelibrary.wiley.com/doi/10.1002/anbr.202100103 by Koc University, Wiley Online Library on [05/09/2026]. See the Terms and Conditions (https://onlinelibrary.wiley.com/terms-and-conditions) on Wiley Online Library for rules of use; OA articles are governed by the applicable Creative Commons License

regions of high-sensitivity zones can be used for density-based analysis and manipulation, as samples with minor density differences ($<0.0023\,g\,m^{-3}$) were stably levitated in the circular regions. The sample levitation positions, in the case of two-ring magnets, become misaligned first and then back to align with the centerline of the container as the separation distance of magnets further increases. Therefore, by controlling this distance, it is possible to identify an extremely high sensitivity region between the magnets ($\approx 87\,500\,mm\,[g\,cm^{-3}]^{-1}$) or to switch to conventional axial MagLev with less sensitivity.[96–98]

Moreover, if the range of density measurement is of importance, it is possible to tilt a standard MagLev design, and therefore tune the gravitational force component relative to the magnetic field (Figure 1E). This simple method offers excellent improvement in density measurement range (from air bubbles ($\rho \approx 0$) to osmium and iridium ($\rho \approx 23\,g\,cm^{-3}$)). However, a MagLev designer should consider the inherent trade-off between measurement range and sensitivity. It is difficult, therefore, to use this method to resolve small differences in density between samples that are both far from the density of the medium (e.g., metals) and physically large enough that they prevent each other, by hard contact, from reaching their equilibrium positions. In addition, by placing the MagLev platform horizontally and using a string to hold samples, it is possible to measure densities of minerals in outdoor explorations with a measurement range of 1.094–9.949 $g\,cm^{-3}$.[101,102]

In standard or two-ring MagLev systems, the sensitivity improves by the reduction of the magnetic field strength (by selecting weaker magnets or increasing their distance) or the paramagnetic medium concentration. However, these may lead to destabilization in density measurement. In the circumstances where measurement sensitivity is of significance, rotating MagLev platforms is useful (Figure 1F). The measurement sensitivity can be improved with flexibility by increasing the rotating speed and eccentric distance of the MagLev setup or by decreasing the paramagnetic medium concentration.[103]

4. Emerging End Applications of Magnetic Levitation

4.1. Proof-of-Concept Particle Levitation

A customized, 3D printed, and lightweight (62 g) MagLev was proposed and integrated with a smartphone to separate microobjects (**Figure 2**).[2] In this setup, a magnification lens (with an outer diameter of 6.33 mm, a numerical aperture of 0.64 mm, and an effective focal length of 4.03 mm) was placed

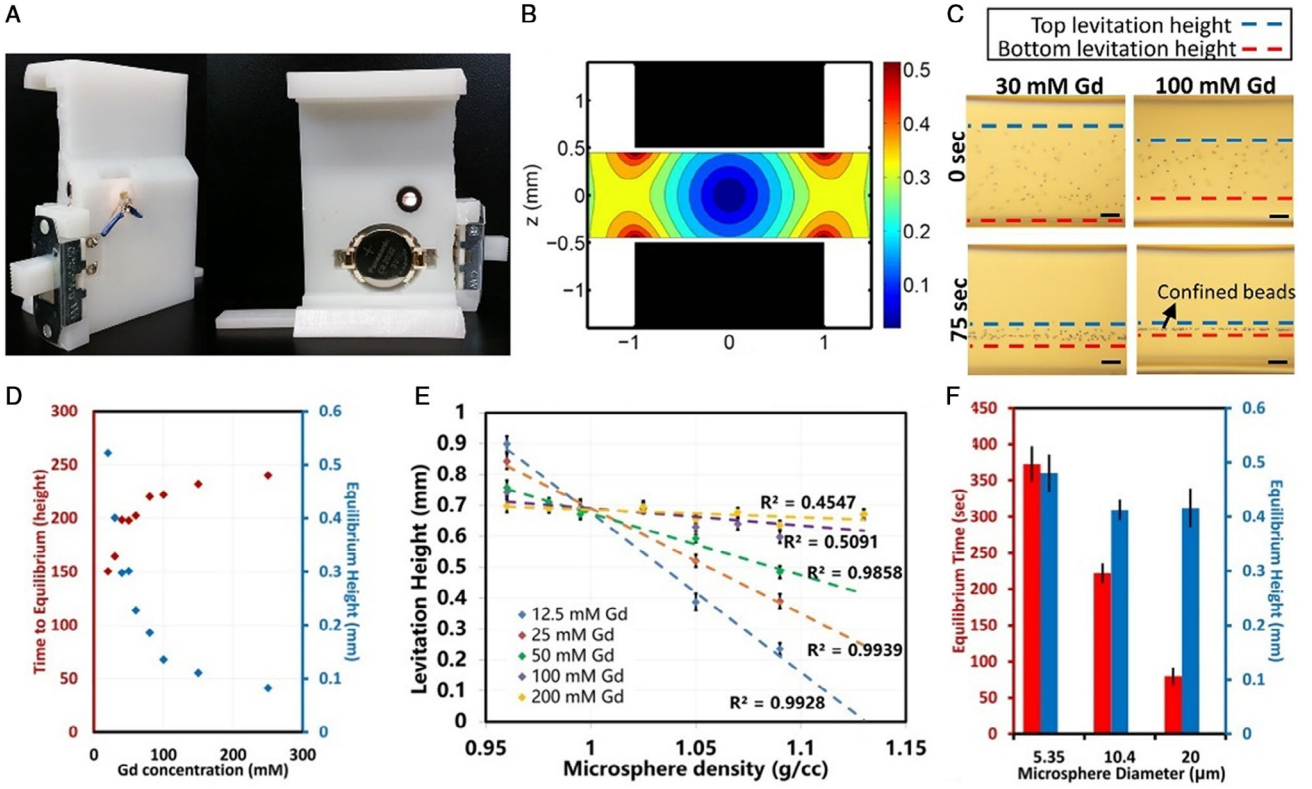


Figure 2. Density-based particle separation using smartphone attachable MagLev. A) The 3D printed case holding the smartphone and capillary tube. B) Illustration of the magnetic field between magnets. C) Levitation of polystyrene microspheres (10 μm) for 0 and 75 s in 30 and 100 mM paramagnetic medium. Confinement limits are presented with red (bottom) and blue (top) dashed lines. D) The equilibrium time (red) and height (blue) in different concentrations of the medium. E) By levitating eight microspheres with standard density, the relation of the density of particles and levitation height was investigated in different concentrations of medium (dashed lines). F) Effects of different microsphere sizes on the equilibrium time (red) and height (blue). The change of particle size had no significant influence on the levitation height.[2] Scale bars are 100 μm. Reproduced under the terms and conditions of the Creative Commons Attribution International license 4.0.[2] Copyright 2015, The Authors, published by PLOS.

© 2021 The Authors. Advanced NanoBiomed Research published by Wiley-VCH GmbH

between the smartphone's camera and a microcapillary ($0.98 \times 0.98\ mm^2$) with micro-objects of various densities suspended in a paramagnetic medium (gadolinium-based (Gd^+)) inside the capillary (Figure 2C). The smartphone images were processed using a custom Android application on the smartphone to calculate the density by levitation height measurements. It was reported that a lower concentration of paramagnetic medium eventuated in more levitation height differences between particles, facilitating the identification of particles with subtle density differences (i.e., better detection resolution) (Figure 2E). Besides, larger microparticles reached the equilibrium height faster than smaller particles (Figure 2F). Image analysis indicated a negative (inverse) linear correlation between the sharpness of the microsphere images and their axial distance, meaning that the resolution dropped as the spheres deviated from the capillary centerline. In addition, the thermal analysis demonstrated that the generated heat by the system (e.g., the smartphone's screen and the light-emitting diode [LED]) did not change the temperature distribution significantly, keeping the density measurements unaffected.[2]

In most of the MagLev platforms, only a single container can be loaded each time, which decreases the high throughput of analysis. The separation of particles in a flowing paramagnetic medium is a promising solution to amplify the sorting yield.[104] To investigate the effect of magnet size and flow rate on the sorting efficiency of micro-objects, a MagLev setup was proposed consisting of a magnification lens (with a diameter of 6.33 mm and a numerical aperture of 0.64 mm) and two NdFeB magnets ($50.8 \times 2 \times 5\ mm^3$) surrounding a capillary containing a gadolinium-based paramagnetic solution.[104] Magnet lengths between 10 and 50 mm, and three flow rates (0.1, 0.25, and 0.75 $\mu L\ s^{-1}$) were tested. It was observed that the separation efficiency increased as the magnet length increased or as the flow rate decreased. Smaller magnets and/or higher flow rates mean a shorter exposure time of particles to the magnetic field, thereby giving them less time to focus and reach an equilibrium height.[104]

4.2. Protein Analysis

In order to identify cellular targets of bioactive small molecules and screen inhibitors of proteins, bioassays involving the binding of proteins to resin-bound small molecules are used. Currently, fluorescent or radioactive labels are mostly in use for on-bead binding assays to quantify the binding of a receptor to its ligand.[47] However, these methods are not label-free and require expensive equipment. A label-free and spectroscopy-free MagLev platform was developed for the analysis of the association of ligands and proteins using porous diamagnetic beads functionalized with covalently bound small molecules.[47] The ligands were immobilized on gel beads, and the proteins of interest were subsequently introduced. As protein–ligand binding occurred, the density of each gel bead changed, allowing quantification of bound protein in MagLev setup with two NdFeB magnets ($50 \times 50 \times 25\ mm^3$). The density changes of proteins were measurable with the accuracy of $\pm 0.0006\ g\ cm^{-3}$ (unaided eye) and $\pm 0.0002\ g\ cm^{-3}$ (using a camera), remarking high sensitivity of MagLev for protein studies. Besides, equilibrium time was found to be proportional to the square of the beads' radius and the initial ligands' concentration. The platform was unable to levitate relatively large proteins (>70 kDa, e.g., antibodies), which can be addressed by designing and synthesizing beads with larger pore sizes.[47]

A MagLev setup was developed for plasma protein density quantification using superparamagnetic iron oxide nanoparticles (SPIONs) ($30\ mg\ mL^{-1}$) functionalized as the paramagnetic medium (**Figure 3**).[45] In this setup, two cubic N42-grade NdFeB magnets ($25.4 \times 25.4 \times 50.8\ mm^3$) with a gap of 2.5 cm were employed. Following levitation of standard polyethylene (PE) microspheres of 1.011, 1.033, and $1.05\ g\ mL^{-1}$, ladder

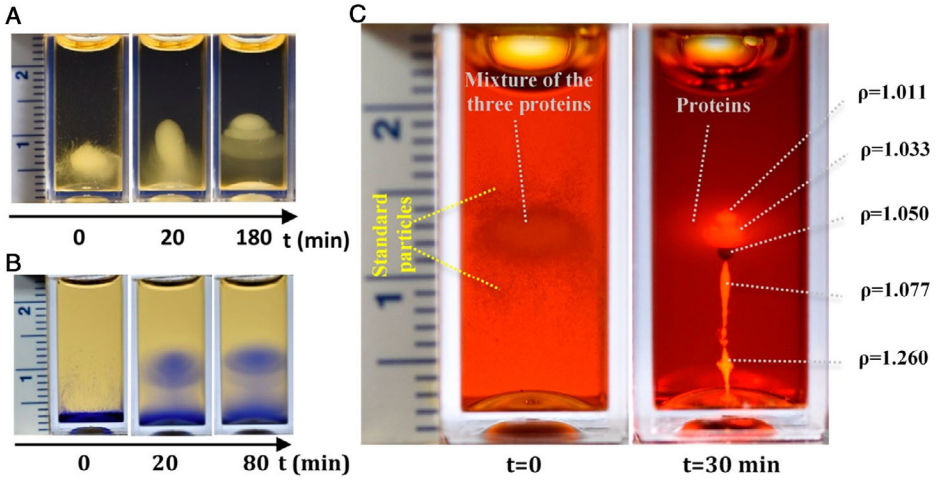


Figure 3. The MagLev design to quantify plasma protein density. A) The emergence of ellipsoidal shapes from plasma proteins as a function of time in $0.06\ mg\ mL^{-1}$ concentration of SPIONs. B) Levitation history of 10-protein ladder in SPION with a concentration of $0.06\ mg\ mL^{-1}$. The molecular mass for these proteins ranged between 9 and 250 kDa. C) Levitation profiles and corresponding densities (in $g\ cm^{-3}$) of a mixture of three proteins (albumin, lysozyme, and immunoglobulin G [IgG]) with different molecular weights mixed with five standard density fluorescent polyethylene microspheres in $1\ mg\ mL^{-1}$ concentration of SPIONs.[45] Reproduced with permission.[45] Copyright 2020, American Chemical Society.

© 2021 The Authors. Advanced NanoBiomed Research published by Wiley-VCH GmbH

26999307, 2022, 3, Downloaded from https://advanced.onlinelibrary.wiley.com/doi/10.1002/anbr.202100103 by Koc University, Wiley Online Library on [05/09/2026]. See the Terms and Conditions (https://onlinelibrary.wiley.com/terms-and-conditions) on Wiley Online Library for rules of use; OA articles are governed by the applicable Creative Commons License

proteins (consisting of standard proteins with known molecular weights) were levitated, and ellipsoidal patterns were seen afterward. It was speculated that these patterns could be related to the structural alternation of single proteins or protein–protein interactions that led to solution structures with higher or lower densities. Finally, three different proteins were levitated with low, middle, and high molecular weight, and five standard fluorescent PE microspheres were employed to calibrate the density measurement. This mixture was levitated at the same height, verifying that the protein density is not a strict function of molecular weights.[45]

MagLev can also detect unlabeled protein–ligand attachment using inexpensive equipment without the need for spectroscopy. In this method, the protein should attach to a small-molecule ligand which was already immobilized on a gel bead. After that, this bead was added to a paramagnetic medium. Then, the diffusion rate of the immobilized protein from the bead into the medium can be determined by monitoring the density change of the gel bead using MagLev. This method could resolve dissociation constants from ≈10 to 100 μM within a relatively short time (20 min–2 h).[48]

For protein detection, a magnetic susceptibility-based MagLev platform was integrated with an inverted microscope for imaging.[37] The principle of magnetic susceptibility is based on labeling the protein with magnetic nanoparticles (MNPs), thus changing the beads' magnetic susceptibility. Generally, polymer microspheres levitate in the midpoint between the two magnets because they have no magnetic susceptibility. However, in the case of binding any magnetically susceptible particles, polymer microspheres would levitate far away from the midpoint and closer to the magnets. This principle was tested to detect the presence of mouse IgG using MagLev. Polymer microspheres (as mobile assay surfaces) and MNPs (as labels) were coated with anti-mouse IgG antibodies that selectively bound with mouse IgG. Once coated particles were introduced into the sample, binding with mouse IgG took place (in the case of the presence of IgG in the sample), forming sandwiches of MNP–antibody–IgG–antibody–microsphere, meaning that the microspheres can be excited in a magnetic field. Using this method, minute changes in the volume magnetic susceptibility of the microspheres were sensed with a resolution of 4.2×10^{-8} per 1 μm of levitation height change. Besides, biotinylated bovine serum albumin in serum was detected with a detection limit of $\approx 110\ \mathrm{fg\ mL^{-1}}$. Furthermore, detection limits of >10 and $1.5\ \mathrm{ng\ mL^{-1}}$ were achieved in serum and buffer, respectively, by developing a sandwich immunoassay for mouse IgG.[37]

A MagLev platform was proposed to study the homogeneity of the created protein corona (PC)-coated NPs through an ex vivo model in order to complement our understanding regarding biological identity therapeutic NPs.[105] Human plasma was used as a protein source, in which polystyrene NPs (60, 100, and 500 nm) were incubated and then placed in a MagLev platform with two NdFeB magnets ($25.4 \times 25.4 \times 50.8\ \mathrm{mm^3}$). The PC-coated NPs levitated around two separate bands inside the paramagnetic medium for all different NP sizes, indicating the heterogeneity of PC. Therefore, it was concluded that contrary to the widely held opinion, the ex vivo method of PC preparation on the surface of model NPs did not result in homogeneous corona formation. Moreover, the results were similar for NPs incubated for 1, 3, and 24 h, describing the independence of incubation time from PC's homogeneity.[105]

4.3. Single-Cell Analysis

MagLev was employed to monitor cells and cellular events. Algae (*Chlamydomonas reinhardtii*), mouse fibroblast (NIH-3T3) (NIH-3T3), and yeast (*Saccharomyces cerevisiae*) were levitated in a 40 mM solution of Gd·DTPA between two permanent magnets, reporting 2.5 μm as the smallest trappable cell size with this platform.[53] In another study, a MagLev platform was developed to measure cell densities as low as $1 \times 10^{-4}\ \mathrm{g\ mL^{-1}}$ using two N52 NdFeB magnets ($50 \times 2 \times 5\ \mathrm{mm^3}$), a microcapillary channel ($50 \times 1 \times 1\ \mathrm{mm^3}$, with a 0.2 mm wall thickness), an inverted microscope, and two mirrors to capture levitation profiles (**Figure 4**A).[106] The density profiles of cancer and blood cells were identified for different cell radiuses, demonstrating a shorter equilibrium time for larger particles (Figure 4B). Moreover, density measurement of 1.025, 1.031, 1.044, 1.064, and $1.089\ \mathrm{g\ mL^{-1}}$ PE particles in 30 mM Gd^{+} was performed in this setup, confirming the ability of MagLev to adequately distinguish subtle density differences on the cellular scale (Figure 4C). Additionally, to study the cell viability in acidic environments, breast cancer cells were studied in control (neutral pH) and acidic (100 mM HCl) microenvironments, which affirmed that acidic environments promote cell sinking (Figure 4D). Finally, to show the density measurement of microorganisms, yeast cells were treated with 100 μM fluconazole and cantharidin, reporting yeast cell resistance to cantharidin and, therefore, small levitation and density change. Moreover, a strong dependency of density to fluconazole was observed, verifying the efficacy of the MagLev platform for microorganism density measurements (Figure 4E).[106]

Hyperplasia and adipocyte hypertrophy are indicators of abnormalities in adipogenesis, which may correlate to diseases such as diabetes, obesity, osteoporosis, and anorexia nervosa.[39] Optical microscopy and flow cytometry are in use for the detection and examination of adipocytes. However, microscopy methods face challenges in terms of separation and manipulation of the cells, and mature cell damages are conceivable in flow cytometry due to the pressure (up to 10 psi). On the other hand, MagLev imposes no pressure on cells while enabling effective manipulation of particles, which can be used for adipocytes and osteoblasts analysis.[107] A MagLev platform was developed to detect bone marrow stem cells (D1 ORL UVA) adipogenic differentiation using a pair of magnets ($50 \times 5 \times 2\ \mathrm{mm^3}$), an inverted microscope, a microfluidic platform, standard beads (for calibration), and two mirrors (placed at 45°).[39] Examining five different concentration of gadolinium (Gd^{3+}), the measurable cell density interval (i.e., detection range) of the system was determined to be $0.956–1.055\ \mathrm{g\ mL^{-1}}$ for 10 mM, $0.882–1.130\ \mathrm{g\ mL^{-1}}$ for 25 mM, $0.760–1.256\ \mathrm{g\ mL^{-1}}$ for 50 mM, $0.637–1.381\ \mathrm{g\ mL^{-1}}$ for 75 mM, and $0.515–1.507\ \mathrm{g\ mL^{-1}}$ for 100 mM Gd^{3+} concentration. The cell density analysis of the adipogenic cohort resulted in $1.079 \pm 0.005\ \mathrm{g\ mL^{-1}}$ on the first day of culture and reduced by 1.76% to $1.060 \pm 0.029\ \mathrm{g\ mL^{-1}}$ on the tenth day. It was reported that adipogenic cells were less dense than stem cells

© 2021 The Authors. Advanced NanoBiomed Research published by Wiley-VCH GmbH

26999307, 2022, 3, Downloaded from https://advanced.onlinelibrary.wiley.com/doi/10.1002/anbr.202100103 by Koc University, Wiley Online Library on [05/09/2026]. See the Terms and Conditions (https://onlinelibrary.wiley.com/terms-and-conditions) on Wiley Online Library for rules of use; OA articles are governed by the applicable Creative Commons License

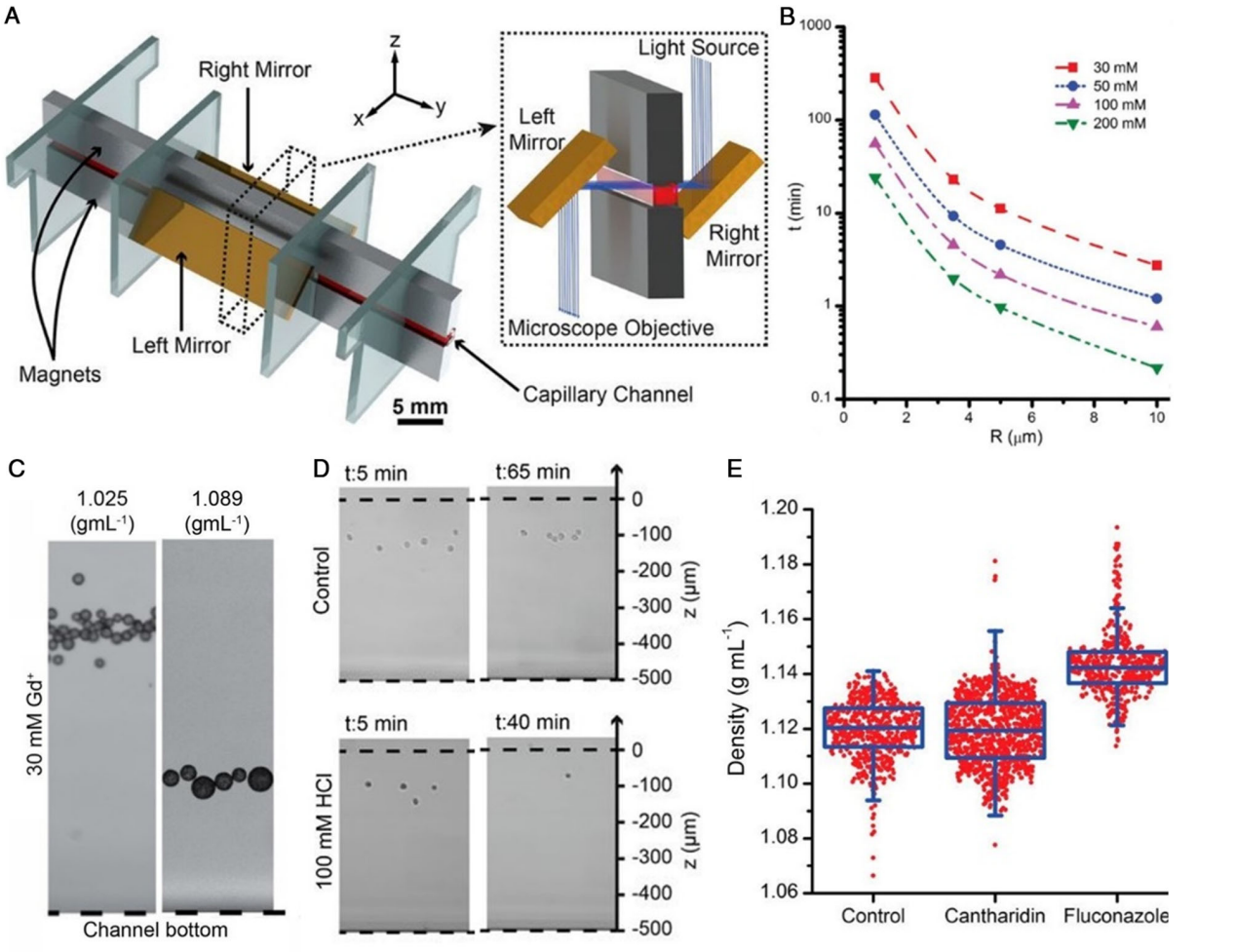


Figure 4. Cell analysis with MagLev. A) Schematic depiction of the platform. Pieces of PMMA are employed to hold platform elements. B) The effect of cell radius on levitation time in different paramagnetic medium concentrations. C) Levitation heights of two standard microparticles in 30 mM Gd. D) Microscopic images of breast cancer cells in control and acidic (100 mM HCl) environments. Cells in acidic environments tend to sink. E) Density distribution of yeast cells treated with 100 μM fluconazole and cantharidin in comparison with the control sample.[106] Reproduced with permission.[106] Copyright 2015, PNAS.

owing to the lipid accumulation inside adipogenic cells during differentiation, reducing their densities and levitating them higher in the microcapillary.[39]

4.4. Blood Analysis and Diseases Diagnosis

4.4.1. Whole Blood, Red Blood Cell, and White Blood Cell Analysis

Integrating high-quality image acquisition capability and ever-increasing computational power of smartphones with MagLev platforms enable robust and semiautomated (with minimal manual steps) analysis of samples with high accuracy, particularly in developing countries.[6] A portable, rapid, label-free, and affordable smartphone-based MagLev diagnostic system (i-LEV) was produced to levitate, separate, and quantify red blood cells (RBCs) and white blood cells (WBCs).[38] A microcapillary channel ($50 \times 1 \times 1\,mm^3$), two N52 NdFeB magnets ($50 \times 2 \times 5\,mm^3$), and side mirrors were used to implement the MagLev platform. In contrast to designs working with manual focusing, the autofocus feature in smartphones could adjust the focal plane without displacing the sample in this device, demonstrating the comparable capability of i-LEV to conventional microscopy. PE beads, RBCs, and WBCs were spiked in phosphate-buffered saline (PBS) containing different concentrations of Gd^+ (30, 60, and 90 mM). Beads with diameters in the range of 10–100 μm and with densities of 1.064, 1.044, 1.031, and $0.125\,g\,mL^{-1}$ were used to verify i-LEV resolution. By imaging and analyzing the width and height of cell bands, the device effectively quantified RBCs spiked in PBS with concentrations in the range of 50–250 million cells mL^{-1}. In addition, it was possible to capture single RBCs at a concentration of 100 000 million cells mL^{-1} and quantify WBC concentrations from 1 to 5 million cells mL^{-1}. Besides, a mobile compatible app could be used so that the end user and healthcare providers could share results and communicate via integrated cloud platforms.[38]

© 2021 The Authors. Advanced NanoBiomed Research published by Wiley-VCH GmbH

26999307, 2022, 3, Downloaded from https://advanced.onlinelibrary.wiley.com/doi/10.1002/anbr.202100103 by Koc University, Wiley Online Library on [05/09/2026]. See the Terms and Conditions (https://onlinelibrary.wiley.com/terms-and-conditions) on Wiley Online Library for rules of use; OA articles are governed by the applicable Creative Commons License

To identify patients with sepsis, MagLev was used to measure the size, morphology, and magnetic properties of circulating leukocytes. It was reported that circulating leukocytes had a substantially higher mean cell area in pixels (px) for infected patients compared with noninfected controls. Median levitation height of circulating leukocytes was measured for 22 infected patients and 39 noninfected control patients, and it was observed that the levitation height was 293.1 ± 61.4 px for septic patients and 288.8 ± 23.7 px for the control group, demonstrating comparable classification performance of the developed MagLev platform.[57]

A smartphone-based MagLev platform capable of detecting soluble and membrane-bound antigens, found in the blood, was developed to detect infectious diseases such as HBV s.a., EBV, HIV, HAV, Dengue, Zika, and Chikungunya.[108] This platform was successful in the detection of T-cell antigen CD3, RBC antigens CD35 and RhD, eosinophil antigen Siglec-8, soluble IL-6, and RBC-bound Epstein–Barr viral particles, while the detection performance was validated with immunofluorescence microscopy. This setup was potent to replace flow cytometry, enzyme-linked immunosorbent assay (ELISA), or microscopy to detect, screen, and quantify different blood pathogens and antigens in resource-limited environments.[108]

To alleviate the relatively slow analysis of MagLev devices, a high throughput method was proposed to levitate and image

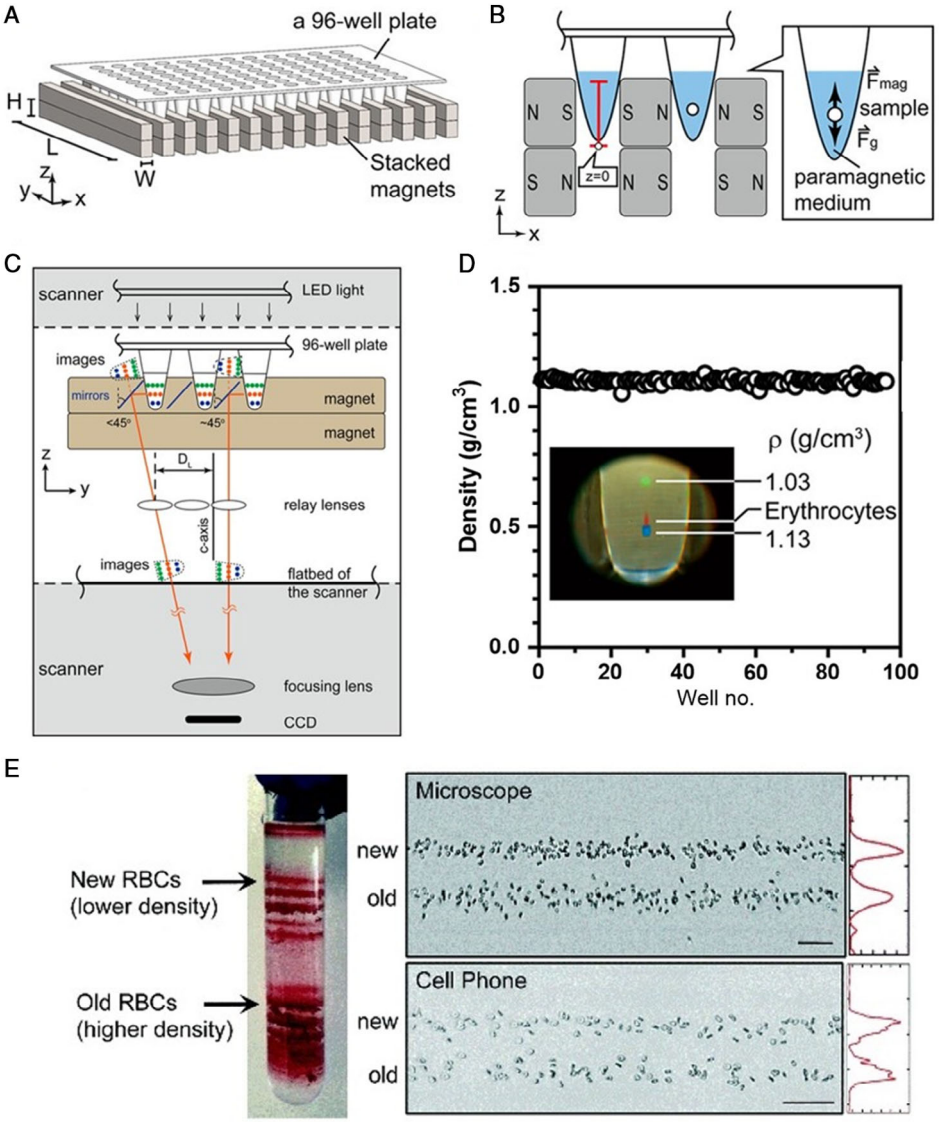


Figure 5. A-D) A high throughput MagLev device based on 96-well plates and a flatbed scanner. A) The schematic of the design. B) The *x*–*z*-plane image of the setup. The red line denotes the magnetic field for sample levitation. C) Key optical components of the design. D) Erythrocyte density measurements. Diluted whole blood was levitated in PBS containing 60 mM gadobutrol. This erythrocyte sample was estimated to have a mean density of 1.10 ± 0.03 g cm^{-3} for $N = 93$ wells, which was in agreement with the value reported in the literature (1.11 g cm^{-3}).[100] Reproduced with permission.[100] Copyright 2018, American Chemical Society. E) Smartphone-based Maglev for blood analysis. (left) RBCs of different ages were separated using centrifugation in Percoll gradient solution. (right) Distinguishable levitation bands for new and old RBCs. Red graphs represent the intensity profiles. All scale bars represent 50 µm.[109] Reproduced with permission.[109] Copyright 2016, Royal Society of Chemistry.

© 2021 The Authors. Advanced NanoBiomed Research published by Wiley-VCH GmbH

26999307, 2022, 3, Downloaded from https://advanced.onlinelibrary.wiley.com/doi/10.1002/anbr.202100103 by Koc University, Wiley Online Library on [05/09/2026]. See the Terms and Conditions (https://onlinelibrary.wiley.com/terms-and-conditions) on Wiley Online Library for rules of use; OA articles are governed by the applicable Creative Commons License

micron-sized samples, including human erythrocytes, using a flatbed scanner, 96-well plates, and particles with standard densities as reference (**Figure 5**A).[100] To realize this design, mirrors were placed in the magnet array gaps and between the tubes (at ≈45°) to transfer images of the tubes down to the scanner. In this setup, 15 pairs of evenly spaced (4.2 mm gaps) magnets ($101.6 \times 4.8 \times 6.4\ mm^3$) were used with the like-poles facing (Figure 5B). To solve the issue of out-of-focus images, an array of relay lenses was employed to focus the images of samples inside wells to the flatbed scanner (Figure 5C). Using this setup, the density of 3-chlorotoluene liquid drops, crystals of cholesterol, and erythrocytes were measured to be 1.069 ± 0.008, 1.030 ± 0.005, and $1.10 \pm 0.03\ g\ cm^{-3}$, respectively, which were in agreement with those reported in the literature, 1.075, 1.067, and $1.11\ g\ cm^{-3}$, respectively (Figure 5D).[100]

To identify and sort cells rapidly (in 15 min), a smartphone-based MagLev platform was proposed.[109] To demonstrate the system performance, beads with known densities and RBCs with artificially altered densities were employed, and a microscope was used for verification purposes. To validate the capabilities of the platform, RBCs were taken from the control (healthy) and anemic patients, and it was found that anemic cells levitated higher due to their lower densities (Figure 5E). Moreover, old and fresh RBCs were successfully separated, indicating that old RBCs were heavier than their fresh counterparts. Comparison of smartphone images and microscope results confirmed a comparable performance.[109]

4.4.2. Cancer

Malignancy and invasiveness of cancer cells can be correlated to the stiffness of the extracellular matrix (ECM), where mechanical signals from the ECM can influence the physical properties of cells (e.g., density).[110] A MagLev device was designed to characterize A549 lung cancer and MDA-MB-231 breast cancer cells based on their density profile after being cultured on 3D hydrogels of increasing collagen concentration (i.e., various fiber densities).[110] Cancer cells were expected to have different densities depending on the collagen concentration. Three different concentrations, namely, 0.36, 0.72, and $1.44\ mg\ mL^{-1}$, were used, representing three different fiber densities. After 7 days of incubation, the platform was calibrated using standard beads, cancer cells were loaded into the setup, imaged using a microscope, and the captured images were processed in MATLAB. Cell culture on collagen gels with higher density ($1.44\ mg\ mL^{-1}$) resulted in a greater range of density values for the MDA-MB-231 cells, while no significant variance with A549 cell lines was reported. Hence, MagLev is a potent platform to characterize cancer cells and assess the effects of ECM conditions on the internal properties of cells.[110]

A label-free microfluidic sorter was developed to separate circulating tumor cells (CTCs) in a continuous flow based on their densities using MagLev.[40] The polydimethylsiloxane (PDMS) microfluidic sorter (fabricated using soft lithography) was placed in between two NdFeB magnets ($50 \times 2 \times 5\ mm^3$). Four mirrors (tilted at 45°) and an inverted microscope facilitated the visualization of the sorter. To demonstrate the device potential to extract CTCs ($<1.06\ g\ mL^{-1}$) from blood cells ($1.09\ g\ mL^{-1}$), cells with densities of 1.06 and $1.09\ g\ mL^{-1}$ with a diameter of 20 μm were simulated using the finite-element method, and their trajectories inside the channel were obtained under a $10\ \mu L\ min^{-1}$ flow. These simulations indicated that a channel length of 50 mm would be enough to direct heavier ($1.09\ g\ mL^{-1}$) cells to the lower outlet and $1.06\ g\ mL^{-1}$ cells to the top one. In fetal bovine serum containing 30 mM Gadavist, particles were prepared with a concentration of 10 000 microparticles mL^{-1}. The sample was then delivered into the sorter with a syringe pump at a flow rate of $10\ \mu L\ min^{-1}$. It was reported that 5.32% of heavier ($1.09\ g\ mL^{-1}$) microparticles mistakenly were sorted through the top outlet. As for the bottom outlet, 7.5% of $1.02\ g\ mL^{-1}$ microparticles erroneously ended up to the lower outlet, highlighting the acceptable accuracy of the proposed MagLev setup for CTC collection.[40]

Another low-cost, portable, and smartphone-based MagLev device was proposed for real-time sorting and quantification of micro-objects (e.g., cancer cells) in fluid flow.[111] To perform 3D printing of this device, three different 3D printers (Objet30 prime Polyjet, MakerBot Replicator fused deposition modeling [FDM], and Formlabs 2 stereolithography [SLA] 3D printers) were used to evaluate multiple printing metrics such as cost, printing time, and resolution (the working principle of these 3D printing techniques can be found elsewhere[112,113]). It was reported that all five parts printed with the Polyjet printer were working correctly, while four pieces of SLA-printed and only two parts of FDM-printed components were working. However, the printing cost of five parts for the Polyjet printer was 30 and 4 times more than that of FDM and SLA printers, respectively. As for the resolution, Polyjet showed the best accuracy among these printers. In addition, the printing time was relatively constant among the three printers, ranging between 25.2 and 28.7 h. Therefore, an optimized combination of the five parts was chosen based on the cost analysis. After print optimization, the device was tested with a mixture of different blood cells and cancer cells suspended in a paramagnetic solution flowing through a magnetic field, reporting a successful separation of lung, prostate, breast, and ovarian cancer cells from blood cells with distinct confinement lines.[111]

An automated MagLev platform with LDIHM was designed for label-free separation of three various cell lines (i.e., MDA-MB-231 [breast cancer cells], D1 [bone marrow stem cells], and U937 [monocytes]) and comparing them to their dead correspondents (**Figure 6**).[50] The imaging was based on interferometry, meaning that the undistorted incoming light and the diffracted light from the sample would meet at the sensor to realize an interference (hologram) pattern. Two N52 NdFeB magnets ($50 \times 2 \times 5\ mm^3$), with a separation gap of <1 mm, were used in a stereolithography-based 3D printed framework. The effect of the concentration of the paramagnetic medium on the levitation height was investigated, reporting that a lower concentration of medium resulted in more difference in the levitation height of particles of different densities (better resolution) while limiting the operational range of the device (Figure 6B). After 10 min of levitation, it was observed that dead cells levitated at lower heights compared to the live cells, demonstrating the ability of the proposed MagLev setup to adequately monitor cell density changes as a result of the loss of viability (Figure 6C,D). Moreover, the effects of three different drug concentrations

© 2021 The Authors. Advanced NanoBiomed Research published by Wiley-VCH GmbH

26999307, 2022, 3, Downloaded from https://advanced.onlinelibrary.wiley.com/doi/10.1002/anbr.202100103 by Koc University, Wiley Online Library on [05/09/2026]. See the Terms and Conditions (https://onlinelibrary.wiley.com/terms-and-conditions) on Wiley Online Library for rules of use; OA articles are governed by the applicable Creative Commons License

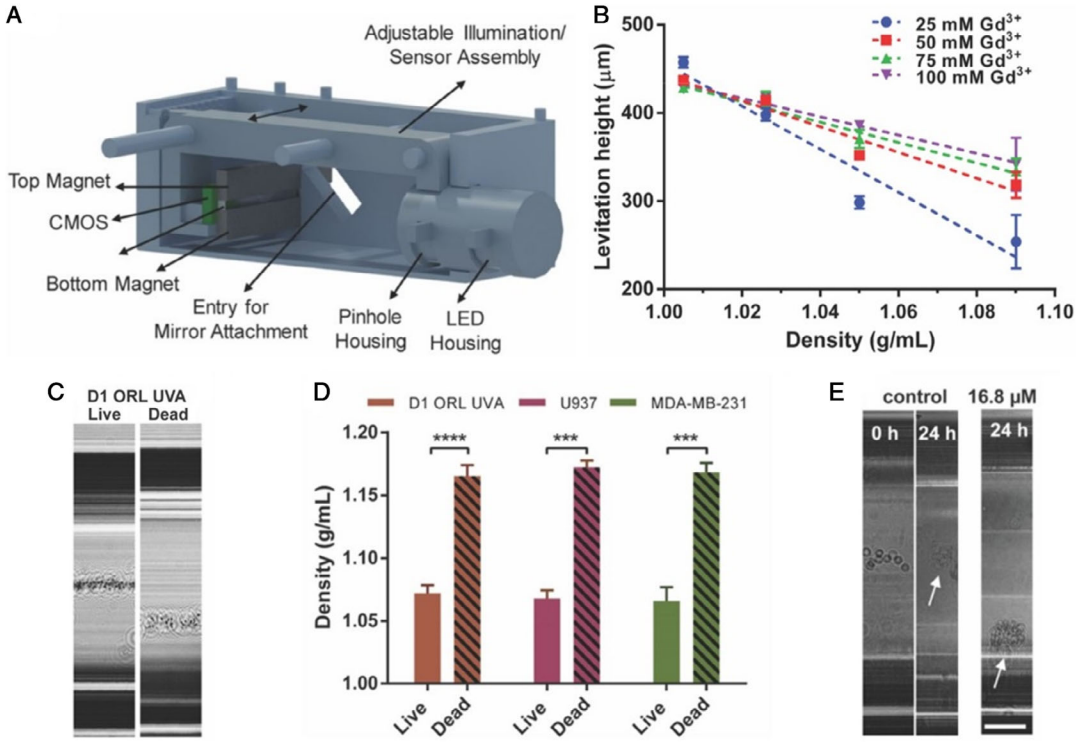


Figure 6. MagLev based on lensless digital inline holographic microscopy. A) Different components of the platform. B) The analysis of the levitation height of various density microspheres for different paramagnetic solution (Gd^{3+}) concentrations (dashed lines are linear fitting at each concentration). C) Levitation height of live and dead D1 ORL UVA cells in 100 mM Gd^{3+}. D) Calculated average densities for different live and dead cells. E) Drug response of MDA-MB-231 cells in 100 mM Gd^{3+} at 16.8 μM doxorubicin concentration during levitation.[50] Reproduced with permission.[50] Copyright 2021, American Chemical Society.

(4.2, 8.4, and 16.8 μM) on cancerous cells were monitored during a period of 24 h. An increase in drug dose resulted in higher cell densities due to cell viability reduction. After 24 h, cell densities were calculated as 1.0621, 1.1608, 1.1531, and 1.2415 g mL^{-1} for control, 4.2, 8.4, and 16.8 μM of doxorubicin, respectively (Figure 6E). However, to use this platform, cell concentration needs to be sufficiently low to reduce the holographic errors (twin images) in spatial positions. With this device, it was possible to acquire high-resolution images (<2 μm) without costly optical platforms, making this tool useful for portable and affordable point of care (PoC) medical applications.[50]

A more advanced smartphone-based MagLev system was used with three microscopy modes, i.e., bright field, dark field, and fluorescence microscopy.[35] A custom-designed 3D printed case was used to hold the smartphone, an aspheric lens with a numerical aperture of 0.64 mm and diameter of 6.33 mm, a capillary tube, two NdFeB magnets ($50.8 \times 2 \times 5$ mm^3), LEDs with different colors, emission filters for both dark-field and bright-field imaging modes, and electronic components to exchange emission filters. Excluding the smartphone, the system weight was 214 g, with a cost of $105.87. Microspheres of various diameters between 5.35 and 79 μm were introduced into a 100 mM paramagnetic solution and then placed into the capillary tube to evaluate the setup performance. It was reported that imaging the sample in bright mode and dark mode gave similar results, demonstrating the ability of the device to capture cell-sized beads. Besides, the best contrast was attainable when the used emission filter, RGB channel, and microspheres had the same color. The setup performance was evaluated for biological applications, cell counting, and concentration determination, using breast cancer cells cultured and stained with calcein in five different concentrations. The concentration of cancer cells was measurable with 10 μL of the sample, obviating the need to acquire large samples from patients. Moreover, the proposed device determined the concentration of cells accurately (a 0.95 linearity) with a detection limit of 680 cells mL^{-1} or 1 cell in 1.47 μL.[35]

4.4.3. Hepatitis C

According to the World Health Organization (WHO), virtually 71 million individuals have chronic hepatitis C virus infection, which caused ≈400 000 deaths in 2016.[114] Although 95% of hepatitis C cases are curable with antiviral medicines, late diagnosis and inadequate treatment increase the chance of developing cirrhosis or liver cancer, particularly in resource-limited settings.[114] MagLev, as a portable and electricity-free method, is a viable candidate for hepatitis C diagnosis in PoC applications. For this purpose, a portable smartphone-assisted MagLev device was developed as a means for PoC detection of hepatitis C virus (HCV), with no external power source and optical instrument required (**Figure 7**A).[58] The setup was composed of a glass microcapillary channel (1×1 mm^2 in cross section, 50 mm in length, with a 0.2 mm wall thickness), two NdFeB magnets ($50.8 \times 6.35 \times 3.175$ mm^3), and four (17×23 mm^2) aluminum-coated flat mirrors. Prior to the HCV identification test, the

© 2021 The Authors. Advanced NanoBiomed Research published by Wiley-VCH GmbH

26999307, 2022, 3, Downloaded from https://advanced.onlinelibrary.wiley.com/doi/10.1002/anbr.202100103 by Koc University, Wiley Online Library on [05/09/2026]. See the Terms and Conditions (https://onlinelibrary.wiley.com/terms-and-conditions) on Wiley Online Library for rules of use; OA articles are governed by the applicable Creative Commons License

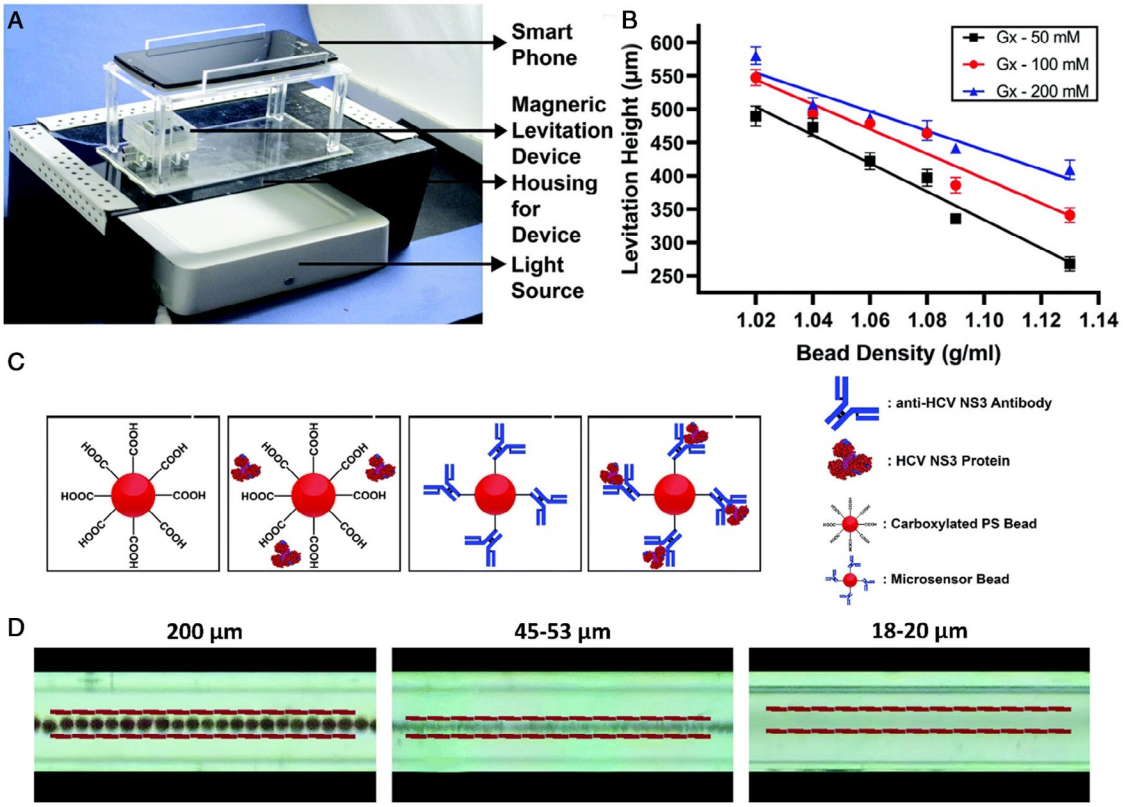


Figure 7. The smartphone-assisted MagLev platform for hepatitis C detection. A) Constituent elements of the platform. B) Levitation resolution of different concentrations of the paramagnetic medium. A higher slope of the line means more difference in levitation heights for small density differences. C) Working principle of hepatitis C detection method using anti-HCV NS3 antibody functionalized beads. D) Imaging resolution of the smartphone camera for different bead sizes.[58] Reproduced with permission.[58] Copyright 2020, Royal Society of Chemistry.

device was calibrated with density markers (polyethylene beads [≈200 µm]) in different paramagnetic agents. Microsensor beads, functionalized with anti-HCV NS3 antibody, were added to the sample to capture the HCV NS3 proteins (if present in the sample) as HCV biomarkers, ultimately increasing the density of functionalized beads in HCV samples compared to beads in the healthy samples (Figure 7C). The platform successfully detected the density difference between nonfunctionalized and anti-HCV NS3 antibody-coated MS beads from a levitation height difference of $\Delta h = 19.17 \pm 0.31$ µm, demonstrating the capability of the proposed setup for HCV detection. Moreover, among tested paramagnetic medium concentrations (50, 100, and 200 mM Gx), the highest detection resolution was reported for the 50 mM Gx (Figure 7B). Without expensive imaging equipment (e.g., microscopes), the smartphone camera was able to take clear images of 200 µm beads, whereas images of 45–53 µm beads were not of high quality, yet suitable for levitation height measurements. Nonetheless, in the smartphone images, 18–20 µm beads appeared as a blurred cloud of particles, in which small density differences were difficult to distinguish (Figure 7D).[58]

Metal-amplified density assay, as a bead-based MagLev assay, is a method for screening the levitation height of polystyrene beads accompanying biomolecules (e.g., proteins, nucleic acids, antibodies, or antigens) on their surfaces. The working principle is based on using gold nanoparticle (AuNP)-labeled biomolecules and electroless deposition of gold or silver.[51] As a result, AuNPs grow in size, and their density change is amplified, making the detection easier. In the case of utilizing antibodies or antigens as recognition elements, the performed assay would be an immunoassay. Based on this methodology, a MagLev setup was proposed with no need for electrical power for two different assays: 1) a quantitative density-linked immunosorbent assay (DeLISA) to quantify neomycin residues in milk, and 2) a multiplexed DeLISA to detect syphilis and hepatitis C in blood serum.[51] Results showed a levitation height of 27 mm for beads exposed to the antibiotic-free milk and a levitation height of 35 mm for beads exposed to the sample with 500 ppb of neomycin, pointing out adequate accuracy of metal-amplified-based MagLev for neomycin analysis. Moreover, beads of different colors were used (e.g., yellow [human IgG, positive control], pink [HCV NS3], and blue [T. pallidum p47]) to reveal the presence of certain antibodies in the sample by changing the levitation height. It was reported that the beads' levitation heights were changed only when the corresponding cognate antibody was present in the serum sample, highlighting the capability of the proposed MagLev platform for syphilis and hepatitis C analysis.[51]

4.5. Sickle Cells

Sickle cell disease (SCD) can be fatal if left undiagnosed. A 3D printed smartphone-based MagLev was proposed to separate

© 2021 The Authors. Advanced NanoBiomed Research published by Wiley-VCH GmbH

26999307, 2022, 3, Downloaded from https://advanced.onlinelibrary.wiley.com/doi/10.1002/anbr.202100103 by Koc University, Wiley Online Library on [05/09/2026]. See the Terms and Conditions (https://onlinelibrary.wiley.com/terms-and-conditions) on Wiley Online Library for rules of use; OA articles are governed by the applicable Creative Commons License

sickle cells with a higher density than normal cells in a small volume of the blood sample with minimal sample preparation required.[41] Smartphone images demonstrated that control (healthy) RBCs levitated higher and had a narrower height distribution. In contrast, sickle cells had a lower levitation height and a wider range. Acquired images with the microscope also corroborated the potency of the device to sort sickle cells effectively.[41] Despite its single-cell and label-free detection capabilities, this device was not able to monitor real-time responses of cells to stimuli such as certain drugs on a particular type of cells.

A self-contained and affordable (less than $100) MagLev was proposed to detect sickle cells in blood samples in a short time (15 min) using a small blood volume (only a drop) by an embedded Raspberry Pi computer running a Python script, with minimal need for user intervention (only reagent mixing) (**Figure 8**).[115] Gd solution and sodium metabisulfite were mixed with the blood sample and delivered inside a capillary tube placed between two NdFeB magnets ($2 \times 5 \times 50\ mm^3$) with a 1.1 mm gap. Polystyrene microspheres and RBCs levitated at the height of 35 and 110 μm for 100×10^{-3} and 25×10^{-3} mM concentration of the paramagnetic medium, respectively, highlighting the capability of self-contained MagLev to effectively levitate and analyze blood samples for sickle cell diagnosis. Moreover, it was reported that a higher detection resolution was achievable using low concentrations of the paramagnetic medium to detect subtle density changes.[115]

4.6. Forensic

In the forensic chemistry field, low concentrations of illegal drugs in minute samples (mass <50 mg) can be challenging to identify and analyze. Among standard portable methods (calorimetric tests, handheld Raman, and Fourier-transform infrared [FTIR] spectroscopy) for general detection of illicit drugs by law enforcement personnel, FTIR-attenuated total reflection (FTIR-ATR) and Raman spectroscopy (which outperform calorimetric tests in sensitivity and accuracy) have a minimum detection threshold of approximately 5 wt%. Therefore, these methods may not be suitable for detecting trace concentrations of drugs inside the mixtures of illegal drugs, adulterants, and diluents.[14] To overcome this difficulty, MagLev was shown promising for identifying undetermined powders in mixtures.

In this regard, a MagLev platform was utilized for initial separation, followed by FTIR-ATR characterization, allowing the detection of fentanyl in a sample of fentanyl-laced heroin (1.3 wt% fentanyl, 2.6 wt% heroin, and 96.1 wt% lactose).[14] A cuvette filled with Gd(DPM)3TOPO (450 mM) was used to perform the separation in a 23 and 77 vol% mixture of hexane and tetrachloroethylene (**Figure 9**A). Using MagLev, this device could capture trace (1.0–2.6 wt%) components from powdered mixtures, i.e., 1) 1.0 wt% lidocaine·HCl and 99.0% caffeine; 2) 1.3 wt% fentanyl·HCl, 2.6 wt% heroin·HCl, and 96.1 wt% α-lactose; and 3) 99.0 wt% lidocaine·HCl and 1.0 wt% caffeine (Figure 9B). This study also indicated that the combination of FTIR-ATR with MagLev was functional for forensic drug inspection because both methods were portable and compatible with powdered compounds. These two methods complement each other because MagLev, by magnetically focusing fentanyl, can achieve higher sensitivity than FTIR-ATR when dealing with complex mixtures.[14]

MagLev was proven successful in characterizing forensic-related evidence for determining densities of gunpowder and glitter samples, separating glitter particles with various densities, and determining the density of a glitter sample extracted from a heterogeneous sample matrix. In a $1 \times 1 \times 4.5\ cm^3$ cuvette containing $MnCl_2$ as the paramagnetic medium, the density of a variety of glitters and gunpowder was measured with MagLev, which ranged from 1.4 to $2.4\ g\ cm^{-3}$ for glitters and from 1.226 to $1.662\ g\ cm^{-3}$ for gunpowder. Also, this device was able to separate a mixture of Chrome Silver 1P and Mirror Crystalina I glitter samples.[60]

MagLev can also be used in forensic evidence processing of rape kits. In line with this, a microchannel with a $1 \times 1\ mm^2$ cross section was inserted between two NdFeB magnets, along with two mirrors located at two sides of the microchannel, improving the resolution of microscopic imaging.[61] Complex mixtures of sperm and E-cells (standing for rape kit forensic samples) were separated under DAPI and bright field microscopy. For sperm concentrations of 100, 500, and 1000 sperm cells per sample volume, the separation efficiencies were reported to be 93.9%, 96.1%, and 94.5%, respectively. In addition, flow-based sorting was performed to direct sperm to the top outlet of the microfluidic capillary (sperm channel) while isolating E-cells to the bottom one. Average sorting efficiencies of 92.3%, 92.2%, and 93.6% were reported after three trials with 10 000 E-cells and 100, 500, and 1000 sperms, respectively. Finally, to validate the technique with samples closest to actual case samples, three mock forensic samples were investigated. Despite the age of the mock samples (from 2003 and 2015), cells exhibited stable levitation heights with a sorting efficiency of $90.4 \pm 0.95\%$ for sperms. By employing MagLev, the processing time was reduced by over 20-fold (i.e., down to 20 min) compared to differential extraction techniques, providing an affordable and high-throughput substitute to the current time-consuming methods.[61]

4.7. Bottom-up Tissue Engineering

3D cell cultures, compared to 2D cultures, recapitulate the complexity of cell behavior in vivo more accurately in terms of drug sensitivity, signaling pathway activity, gene expression profiles, cell–cell and cell–matrix interactions.[116–118] Traditional 3D cell culturing involves a process called the top-down approach, where cells are seeded into a porous scaffold to create the desired tissue. However, in bottom-up or modular approaches, small modules of cells are assembled to make large tissues with the aid of modular scaffolds, overcoming the top-down approach limitations such as low cell density, limited diffusion, and slow vascularization.[119] However, using scaffolds has its drawbacks, such as the inhomogeneity of cells inside the scaffold,[120] the need for scaffold synthesis and sterilization,[121] and the limited selection of biocompatible material.[122] Furthermore, 3D bioprinting is an emerging method for the rapid prototyping of perfusable, complex 3D bioconstructs (ranging from organ-on-chip to full-scale organs).[123–126] However, due to the high shear stress or intense light exposure, retaining cell viability during the printing process is challenging.[124,127]

© 2021 The Authors. Advanced NanoBiomed Research published by Wiley-VCH GmbH

26999307, 2022, 3, Downloaded from https://advanced.onlinelibrary.wiley.com/doi/10.1002/anbr.202100103 by Koc University, Wiley Online Library on [05/09/2026]. See the Terms and Conditions (https://onlinelibrary.wiley.com/terms-and-conditions) on Wiley Online Library for rules of use; OA articles are governed by the applicable Creative Commons License

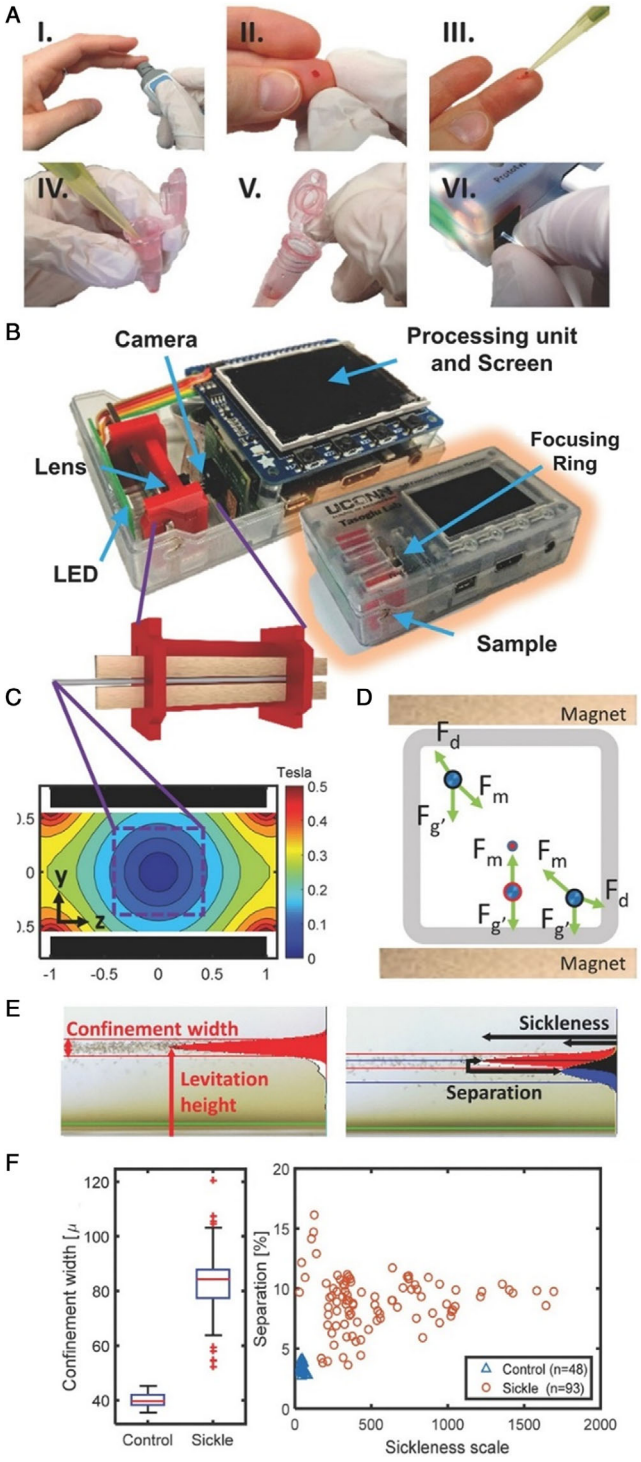


Figure 8. Label-free sickle cell analysis with self-contained MagLev. A) Steps of sample preparation. B) Inside of the device. Magnets, lens, LED, and a built-in camera were the main components of the device. C) The magnetic field acting on the cross section of the capillary tube. D) Different forces exerted on an object in the paramagnetic medium. F_m, magnetic force; F_g, gravitational force; F_d, drag force; and F_b, buoyant force. At the stable equilibrium condition, F_d is zero, where F_m and F_g' are equal and in opposite directions. E) (left) Levitation height and confinement width of RBCs. (right) Separation means the normalization of the discrepancy between the average levitation heights to the greater mean value, while sickleness means the ratio between the normal fit heights. (F) (left) Confinement width of control RBCs and SCD RBCs obtained experimentally (i.e., the total width of two Gaussian curves fit pixel intensity gradient data. (right) Representing experimental results for separation and sickliness percentage for the same control and SCD depicted in the left figure.[115] Reproduced with permission.[115] Copyright 2016, Wiley-VCH.

© 2021 The Authors. Advanced NanoBiomed Research published by Wiley-VCH GmbH

26999307, 2022, 3, Downloaded from https://advanced.onlinelibrary.wiley.com/doi/10.1002/anbr.202100103 by Koc University, Wiley Online Library on [05/09/2026]. See the Terms and Conditions (https://onlinelibrary.wiley.com/terms-and-conditions) on Wiley Online Library for rules of use; OA articles are governed by the applicable Creative Commons License

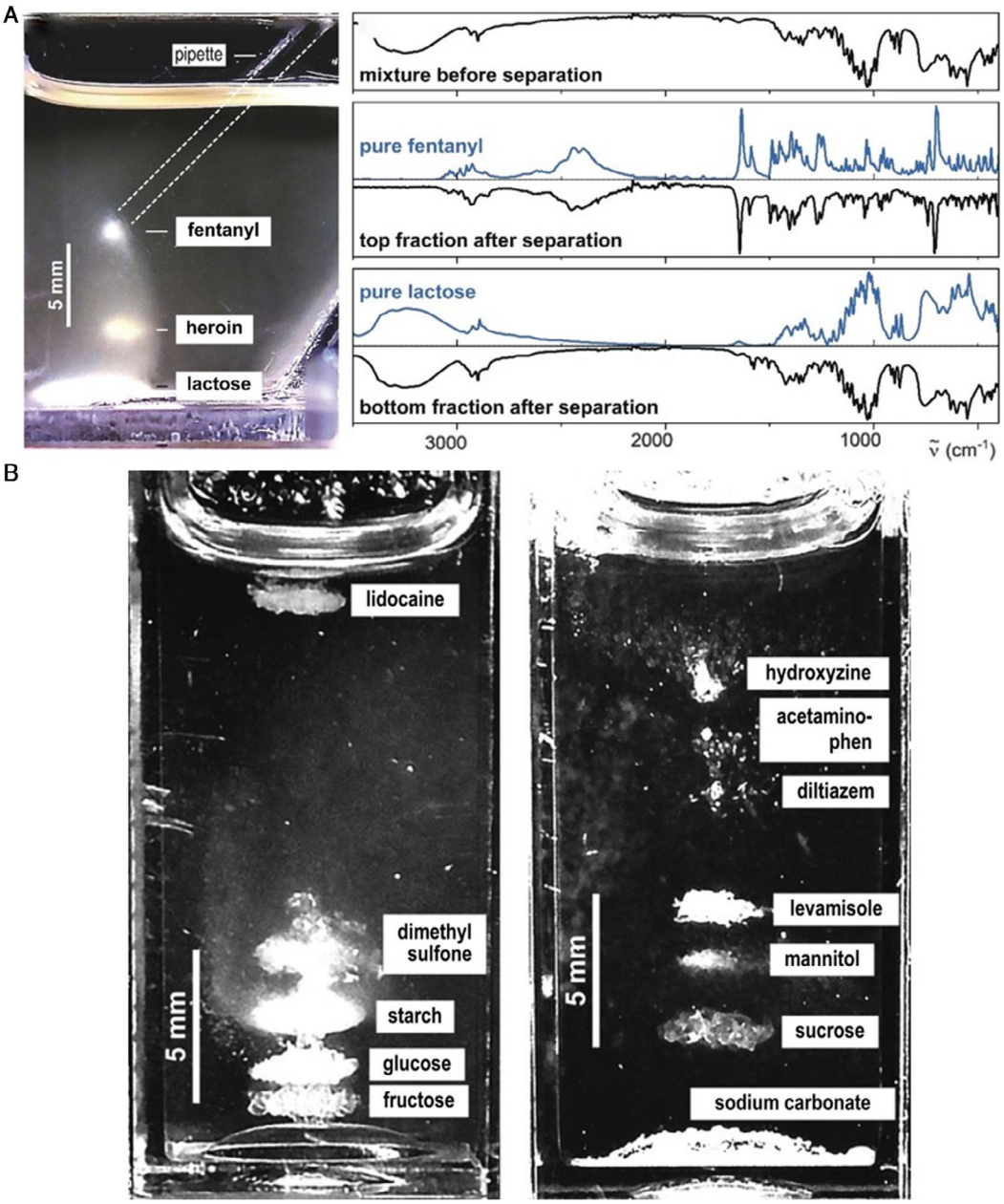


Figure 9. The application of MagLev in forensic analysis. A) Separation and identification of trace fentanyl in a mixture containing heroin and lactose using. (left) The separation of a powdered mixture of fentanyl-containing heroin (fentanyl·HCl (1.3 wt%), heroin·HCl (2.6 wt%), and α-lactose (96.1 wt%)) using MagLev after 30 min of levitation. (right) The separated constituents were removed, rinsed, and air-dried. Black lines represent FTIR-ATR spectra for the unprepared mixture (top) and the separated fractions (bottom) containing fentanyl and lactose. Pure compounds correspond to the blue lines. B) Final (end time) images of the MagLev separation of mixtures containing drugs, adulterants, and dilutants with Gd(DPM)3TOPO (450 mm) as the paramagnetic medium.[14] Reproduced with permission.[14] Copyright 2020, Wiley-VCH.

Although electromagnets are in use for levitation, manipulation, alignment, and assembly of ferromagnetic particles, only materials with strong magnetic properties (containing Ni, Co, and/or Fe) can be suspended. MagLev (which suspends diamagnetic objects), on the other hand, can be used to address the abovementioned limitations, enabling contactless orientation/manipulation of fragile biomaterial and scaffold-free assembly of bioconstruction.[128] In this approach, first, microcomponents (e.g., cells) should be suspended and oriented in desired layer-by-layer order (as a result of an equilibrium between gravitational, buoyant, and magnetic force), and then the assembly is done by gradual draining of the paramagnetic medium (**Figure 10**).[128] Assembling cell structures by MagLev is advantageous because it does not induce any toxic or inflammatory response, and no electrical power is needed for levitation.[65]

A proof-of-concept MagLev platform was developed based on magnetic NP assembly to model white adipose tissue (WAT) and

© 2021 The Authors. Advanced NanoBiomed Research published by Wiley-VCH GmbH

26999307, 2022, 3, Downloaded from https://advanced.onlinelibrary.wiley.com/doi/10.1002/anbr.202100103 by Koc University, Wiley Online Library on [05/09/2026]. See the Terms and Conditions (https://onlinelibrary.wiley.com/terms-and-conditions) on Wiley Online Library for rules of use; OA articles are governed by the applicable Creative Commons License



Figure 10. Contactless assembly of particles using MagLev. A) Assembly of four circles and a circular base. Scale bars are 5 mm in length.[128] Reproduced with permission.[128] Copyright 2011, Wiley-VCH. B) Assembly of levitating spheres ordered by colevitating templates. The template, in gray, is shown schematically along with the placement of spheres. The scale bars are 6.3 mm.[150] Reproduced with permission.[150] Copyright 2011, Royal Society of Chemistry.

monitor the culture process using inverted microscopy.[129] Compared to 2D cultures, 3D WAT cultures showed long-term viability for 3T3-L1 preadipocytes, while 2D cultures lost their adherence and cells died after reaching confluence. Additionally, upon adipogenesis induction in 3T3-L1 adipospheres, large lipid droplets formed in 3D cultures (which are typical of white adipocytes in vivo), while only smaller droplets formed in the 2D cultures, and those droplets accumulated more efficiently in 3D cultures, allowing for better intercellular signaling. Besides, the produced 3D structures enabled the formation of vascular-like networks, enabling a robust cell proliferation.[129]

A MagLev platform was designed to create scaffold-free 3D cell cultures, where two $2 \times 2 \times 20\,mm^3$ magnets of $\approx 0.4\,T$, an inverted microscope, and mirrors were used (**Figure 11**A).[130] Instead of MNPs, the cells were magnetized using three different types of chelates of gadolinium (III) paramagnetic agent, namely, gadobutrol, gadoteric acid, and gadodiamide. Two different types of cells were used separately, i.e., NIH 3T3 mouse fibroblast cells and HCC827 non-small cell lung cancer cells, to investigate the ability of the platform to create the desired 3D structures. Evaluating gadolinium (III) chelates, gadobutrol yielded the maximum cell viability compared to the other two chelates, mostly due to its low toxicity, facilitating cell interactions (Figure 11B,C). Besides, the growth rate of cells (number of cells per time) in MagLev-based culture was compared to conventional 2D culture, pointing out an exponential growth for 3D culture and a linear growth for standard 2D culture (Figure 11D).[130] In a similar setup, 3D cell cultures of bone marrow stem cells and breast cancer cells were performed using a different paramagnetic medium. It was reported that compared to a linear ligand containing agents, utilization of macrocyclic ligand containing agents (Gd-BT-DO3A and Gd-DOTA) resulted in higher cell viability.[64] Another similar setup was used to find the effects of paramagnetic medium concentration, culture time, and cell seeding density on 3D cell culturing using mouse fibroblast cells and five different types of cancer cells (HeLa [human epithelial cervix adenocarcinoma], PC-12 [rat adrenal gland pheochromocytoma], SH-SY5Y [human bone marrow neuroblastoma], MDA-MB-231 [human epithelial breast adenocarcinoma], and MCF7 [human epithelial breast adenocarcinoma]).[131] It was reported that the circularity, area, and size of the spheroids could be controlled by manipulating cell culturing time, paramagnetic agent concentration, and cell seeding density. An increase of culture time resulted in the formation of a spheroid with larger

© 2021 The Authors. Advanced NanoBiomed Research published by Wiley-VCH GmbH

26999307, 2022, 3, Downloaded from https://advanced.onlinelibrary.wiley.com/doi/10.1002/anbr.202100103 by Koc University, Wiley Online Library on [05/09/2026]. See the Terms and Conditions (https://onlinelibrary.wiley.com/terms-and-conditions) on Wiley Online Library for rules of use; OA articles are governed by the applicable Creative Commons License

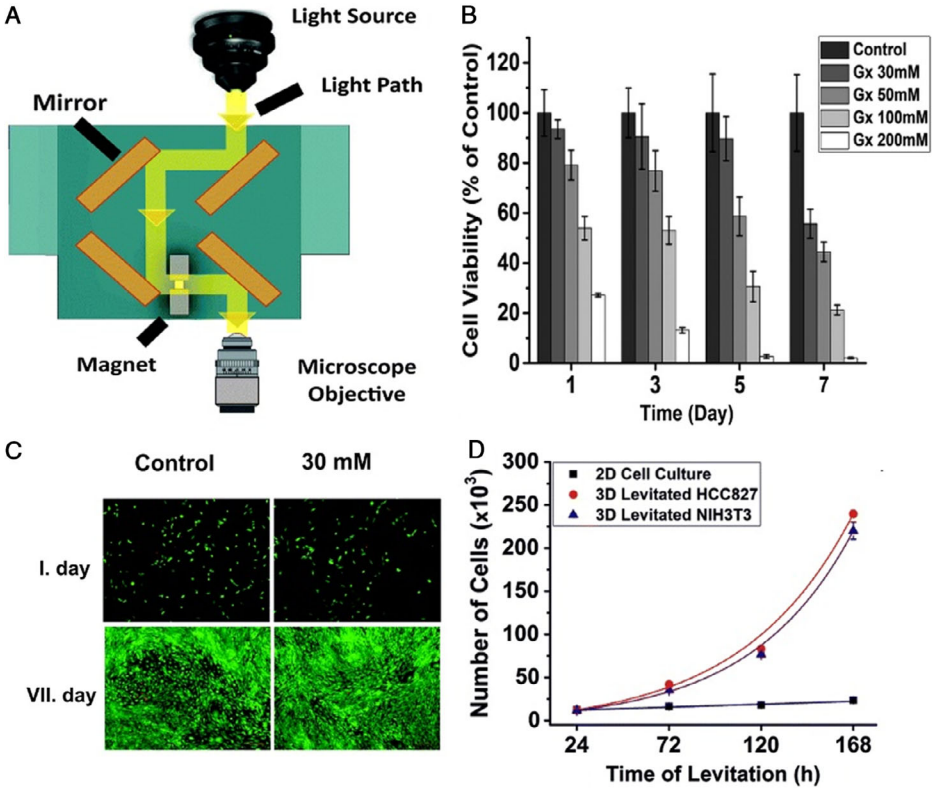


Figure 11. Scaffold-free cell culture using MagLev. A) Constituent elements of the platform. B) Effects of different concentrations of gadolinium chelates on the cell viability. C) Comparison of the cell growth after 7 days for the control and magnetized cultures. D) The cell growth rate was exponential for MagLev-based 3D cell culture, while 2D culture had a lower growth rate, confirming the potency of MagLev for scaffold-free 3D cell cultures.[130] Reproduced with permission.[130] Copyright 2018, Royal Society of Chemistry.

diameters, ultimately decreasing cell viability due to the diffusion limitation (i.e., cell viability decreased from 92%, on day 3, to 58%, on day 7). Besides, a higher concentration of paramagnetic medium (100 mM) brought about a larger area and faster coculture assembly. According to the results, an increase of the cell seeding density, from 5×10^3 to 50×10^3, decreased cell viability below 50% due to the limited nutrients as well as O_2 diffusion inside the spheroid and insufficient mass transport, which caused the accumulation of metabolic waste. Overall, the platform provided an easy-to-use and low-cost method to form 3D cell cultures for 3D bioprinting, regenerative medicine, and drug screening applications.[131]

MagLev was used to culture a scaffold-free 3D breast cancer model in vitro in order to investigate homotypic as well as heterotypic cell–cell interactions, tumor–fibroblast interactions, and effects of tumor microenvironment on drug efficacy.[132] Doxorubicin (100 nM), a chemotherapy drug, was applied to the coculture of cancer cells and fibroblast, which resulted in an 80% and 45% decrease in the area and density of cancer cell culture, respectively, resembling in vivo findings and demonstrating the suitability of MagLev cell cultures for cancer drug studies. In order to study the effects of fibroblast content on drug penetration into tumors, different ratios of breast tumor cells and fibroblasts were examined (50:50 [cell%:fibroblast%], 30:70, 70:30, and 100% fibroblasts), showing that a lower percentage of fibroblast cells resulted in ≈10% higher drug penetration.[132]

In addition to creating 3D cultures of cells and tumors, MagLev can be used to model body organs. An aortic valve was cultured for 3 days in a MagLev platform using valvular interstitial cells (VICs) and valvular endothelial cells (VECs).[133] It was reported that the phenotype was preserved because aortic valve cocultures (AVCCs) stained positive for CD31 and α-smooth muscle actin (αSMA). Besides, the gene expression was decreased for collagen type I, laminin, and fibronectin proteins in 3D compared to 2D, while ECM components also stained positive. The AVCCs thickness was virtually 500 μm after culture. It was suggested that AVCC could be used in the future for mechanobiology and calcific aortic valve disease progression studies.[133]

5. Challenges of Implementing MagLev Systems

MagLev has proven its potential as an innovative technology for contactless manipulation, power-free levitation, and separation of a wide range of diamagnetic objects. Yet, as an emerging technology, MagLev faces unaddressed challenges. First, the magnetic field is applied to all suspended objects without the ability to exert an adjustable magnetic force on a particular object independent of others.[128]

Furthermore, there is a negative correlation between detection resolution (sensitivity) and detection range (dynamic range). A higher concentration of paramagnetic medium applies higher

© 2021 The Authors. Advanced NanoBiomed Research published by Wiley-VCH GmbH

26999307, 2022, 3, Downloaded from https://advanced.onlinelibrary.wiley.com/doi/10.1002/anbr.202100103 by Koc University, Wiley Online Library on [05/09/2026]. See the Terms and Conditions (https://onlinelibrary.wiley.com/terms-and-conditions) on Wiley Online Library for rules of use; OA articles are governed by the applicable Creative Commons License

magnetic force, resulting in faster equilibrium time and a wider range of detectable densities, while shifting levitation height of particles toward the centerline, which compromises detection resolution (i.e., subtle density differences are not distinguishable).[59] Besides, an increase of the magnetic field strength and its gradient can widen the dynamic range while reducing the sensitivity. On the other hand, the use of weaker magnets or increasing the distance between magnets (weakening the magnetic field) improves sensitivity.[134] Moreover, a MagLev platform can be tilted (relative to the gravitational vector) to tune the detection range (by $\approx 15\times$) at the cost of sensitivity.[31] Therefore, MagLev design is a trade-off between resolution and dynamic range based on the application; whether high sensitivity is required (e.g., cell or protein analysis), or a wider dynamic range is of interest (e.g., separation of metallic and polymer particles).[1,31]

In addition, the biocompatibility of the paramagnetic medium is important to retain the viability of biological samples (e.g., cells), particularly in long-term experiments.[45] For instance, denaturation of proteins happens in widely used paramagnetic mediums, such as $GdCl_3$, $MnCl_2$, and $MnBr_2$.[45] Hence, a paramagnetic medium should be selected based on the application and objects to be levitated. In this regard, different families of paramagnetic material have been reported in the literature with different characteristics, such as 1) aqueous solutions of biocompatible chelates of Mn^{II} and Gd^{III} that are useful for biological applications (e.g., cellular and protein assays), 2) aqueous solutions paramagnetic salts (e.g., solutions of $GdCl_3$ or $MnCl_2$) that are suitable for water-insoluble samples, 3) nonaqueous solutions of salts (soluble in alcohols) including $MnCl_2$ and $GdCl_3$ which are less dense compared to water, suitable for suspending object less dense than water (e.g., polyethylene and polypropylene), 4) paramagnetic ionic liquids (PILs) which possess negligible vapor pressures, low melting points, and high thermal stabilities, and 5) phase-separated paramagnetic media.[1,5,33,53,106,135] Although a higher concentration of paramagnetic medium results in a wider detection range, increasing the salt concentration in the medium causes cell dehydration through osmosis, leading to cell density changes (inaccurate readouts) and cell death.[134] Utilization of a secondary container of known density (e.g., a hollow transparent sphere) to isolate/protect cells from direct contact with the medium can be a promising solution.[134]

Environmental parameters, such as temperature and humidity, along with gradual evaporation of the paramagnetic medium solvent, could result in false readouts. However, the use of density standards affords an absolute measure of density regardless of variations of experimental conditions in different laboratories. Furthermore, the presence of air bubbles on levitated objects results in the misleading readout, as air is less dense than the majority of levitated objects of interest. For nonbiological particles, adding a detergent and quickly sonicating the solution can reduce the errors.[60]

In addition, MagLev platforms are relatively low-throughput devices.[1] In most of the designs so far, a single container can be loaded into the platform for levitation and analysis.[1] Besides, smaller objects take a longer time ($\approx$2–24 h for most cells and bacterial species) to reach equilibrium due to the dominant Brownian motion, limiting the high throughput of MagLev devices.[134] A number of viable methods to decrease the equilibrium time are the following: increasing the magnetic field strength, augmenting the concentration of the paramagnetic medium, decreasing the working temperature, reducing the distance traveled by the objects during levitation (i.e., smaller MagLev platforms), and gentle injection of objects into the medium to prevent dispersion.[134] In addition, the integration of MagLev with microfluidic chips[136–141] and multiplexed biomedical platforms[126,142–145] enables the development of flow-assisted devices for real-time monitoring and continuous separation of samples.

Following the suspension of objects, the levitation heights should be quantified either with the naked eye or by imaging equipment. Although a ruler is enough for measuring levitation height in large MagLev setups, advanced imaging methods (e.g., microscopy) are needed for smaller setups levitating submillimeter objects (e.g., cells).[6] Optical, fluorescent, and inverted microscopy techniques are widely used imaging approaches for this purpose. Nonetheless, relatively large size, high cost, demanding external power source, and requiring expert operators are challenges confining portability and affordability, particularly in resource-limited settings.[35] Recent advancements in the image acquisition capability of smartphones enabled imaging of cells and bacteria without microscopes, introducing more portable, user-friendly, and affordable MagLev platforms.[35,41] However, smartphone-based MagLev devices face the challenge of standardization of the platform for different smartphones with different camera characteristics and operating systems.[59] Although self-contained MagLev systems can address these challenges using an embedded camera, an extra image storage and controller board are needed in these platforms.[59,115]

6. Conclusion and Future Perspective

MagLev offers advantages such as 1) being simple in design and use with virtually no maintenance required (except for occasional calibration), 2) being electricity-free which is beneficial for resource-limited settings, 3) being label-free, 4) using cost-effective, commercially available magnets and paramagnetic mediums, 5) being able to levitate/separate/sort multiple objects simultaneously, 6) requiring a small amount of sample which is important for samples that are difficult/painful to obtain (e.g., biological samples/biopsies) or scarce (forensic samples), 7) being compatible with fragile samples (e.g., gels and cells), 8) being insensitive to physical properties of particles (e.g., shape, size, viscosity, elasticity, and stiffness), and 9) being compatible with smartphones to produce portable MagLev platforms with no need to microscopic imaging.[6,100,146]

Size, shape, and strength of magnets, type and concentration of the paramagnetic medium, and the imaging method (e.g., visual, microscopy, smartphone-assisted, or self-contained lenses) are decisive factors determining the performance of MagLev designs (e.g., detection resolution and dynamic range). In the present review, MagLev platforms were discussed from a design perspective, and in order to provide an insight into the opportunities offered by MagLev and current challenges of implementing them, the most recent biomedical end applications of MagLev were presented, such as separation of different

© 2021 The Authors. Advanced NanoBiomed Research published by Wiley-VCH GmbH

26999307, 2022, 3, Downloaded from https://advanced.onlinelibrary.wiley.com/doi/10.1002/anbr.202100103 by Koc University, Wiley Online Library on [05/09/2026]. See the Terms and Conditions (https://onlinelibrary.wiley.com/terms-and-conditions) on Wiley Online Library for rules of use; OA articles are governed by the applicable Creative Commons License

types of cells, detection of cancer cells, blood analysis, and diagnostic applications. Addressing current challenges and integrating with emerging technologies can further extend the applications of MagLev.

Image acquisition and interpretation are complementary steps following levitation. Classification, analysis, and quantification of a large amount of obtained data (either from high-throughput microscopes or smartphone cameras) can outpace human experts with a propensity for biased decisions. Although a number of proposed smartphone-assisted MagLev platforms utilized smartphones for data analysis through predefined software, levitation of undefined objects may challenge the performance of the device. Machine learning (ML) algorithms allow MagLev setups to adapt themselves to new experiments without being explicitly programmed for that specific application.[147,148] Furthermore, we foresee that future studies may employ MagLev to simulate and monitor the possible effects of prolonged weightlessness on the human body (e.g., bone mass loss), which occurs in astronauts who were in zero-gravity conditions for a long period.[149]

Acknowledgements

S.T. acknowledges Tubitak 2232 International Fellowship for Outstanding Researchers Award (118C391), Alexander von Humboldt Research Fellowship for Experienced Researchers, Marie Skłodowska-Curie Individual Fellowship (101003361), and Royal Academy Newton-Katip Çelebi Transforming Systems Through Partnership award (120N019) for financial support of this research. This work was partially supported by Science Academy's Young Scientist Awards Program (BAGEP), Outstanding Young Scientists Awards (GEBİP), and Bilim Kahramanlari Dernegi The Young Scientist Award.

Open Access funding enabled and organized by Projekt DEAL. [Correction added on March 24, 2022, after first online publication: Projekt DEAL funding statement has been added.]

Conflict of Interest

The authors declare no conflict of interest.

Keywords

density-based separation, image cytometry, magnetic cytometry, magnetic levitation, magnetophoresis

Received: August 30, 2021
Revised: October 28, 2021
Published online: December 8, 2021

[1] S. Ge, A. Nemiroski, K. A. Mirica, C. R. Mace, J. W. Hennek, A. A. Kumar, G. M. Whitesides, *Angew. Chem. Int. Ed.* **2020**, *59*, 17810.
[2] S. Knowlton, C. H. Yu, N. Jain, I. C. Ghiran, S. Tasoglu *PLoS One* **2015**, *10*, e0134400.
[3] M. B. Atkinson, D. K. Bwambok, J. Chen, P. D. Chopade, M. M. Thuo, C. R. Mace, K. A. Mirica, A. A. Kumar, A. S. Myerson, G. M. Whitesides, *Angew Chem.* **2013**, *125*, 10398.
[4] K. A. Mirica, S. T. Phillips, S. S. Shevkoplyas, G. M. Whitesides, *J. Am. Chem. Soc.* **2008**, *130*, 17678.
[5] A. Winkleman, R. Castillejos-Perez, K. L. Gudiksen, S. T. Phillips, M. Prentiss, G. M. Whitesides, *Anal Chem.* **2007**, *79*, 6542.
[6] M. M. Alseed, S. R. Dabbagh, P. Zhao, O. Ozcan, S. Tasoglu, *Adv. Opt. Technol.* **2021**, *10*, 109.
[7] H. Fehlauer, H. Wolf, *Meas. Sci. Technol.* **2006**, *17*, 2588.
[8] G. Spedding, *Brewing Materials and Processes*, Academic Press, Cambridge, Massachusetts **2016**, pp. 123–149.
[9] J. Xie, P. Zhao, C. Zhang, J. Fu, L.-S. Turng, *Sens. Actuators, B Chem.* **2021**, *333*, 129533.
[10] A. K. Bryan, V. C. Hecht, W. Shen, K. Payer, W. H. Grover, S. R. Manalis, *Lab Chip* **2014**, *14*, 569.
[11] J. Yang, Y. Huang, X. B. Wang, F. F. Becker, P. R. Gascoyne, *Biophys. J.* **2000**, *78*, 2680.
[12] W. Waheed, O. Z. Sharaf, A. Alazzam, E. Abu-Nada, *J. Chromatogr. A* **2020**, *1637*, 461799.
[13] C. Q. Zhang, P. Zhao, J. Xie, N. Xia, J. Z. Fu, *J. Zhejiang Univ. Eng. Sci.* **2018**, *52*, 613.
[14] C. K. Abrahamsson, A. Nagarkar, M. J. Fink, D. J. Preston, S. Ge, J. S. Bozenko, G. M. Whitesides, *Angew. Chem. Int. Ed. Engl.* **2020**, *59*, 874.
[15] Y.-G. Sun, S. Xie, J.-Q. Xu, G.-B. Lin, *Appl. Sci.* **2020**, *10*, 1179.
[16] J. Ding, X. Yang, Z. Long, N. Dang, *IEEE Access* **2018**, *6*, 61547.
[17] R. Nasiri-Zarandi, A. Hekmati, presented at *2019 Int. Power System Conf. (PSC)*, IEEE Tehran, Iran **2019**.
[18] Z. Ke, D. Zhang, Y. Li, N. Wang, presented at *2008 IEEE Vehicle Power and Propulsion Conf.*, IEEE, Piscataway, NJ **2008**.
[19] W. Braunbek, *Z Phys.* **1939**, *112*, 753.
[20] R. D. Waldron, *Rev. Sci. Instrum.* **1966**, *37*, 29.
[21] I. Simon, A. G. Emslie, P. F. Strong, R. K. McConnell Jr, *Rev. Sci. Instrum.* **1968**, *39*, 1666.
[22] I. Simon, *Google Patents*, **1969**.
[23] U. Andres, *Magnetohydrodynamic & Magnetohydrostatic Methods of Mineral Separation*, John Wiley & Sons, Hoboken, NJ **1976**.
[24] Y. Ikezoe, N. Hirota, J. Nakagawa, K. Kitazawa, *Nature* **1998**, *393*, 749.
[25] E. Beaugnon, R. Tournier, *Nature* **1991**, *349*, 470.
[26] A. Catherall, L. Eaves, P. King, S. Booth, *Nature* **2003**, *422*, 579.
[27] M. Sagawa, S. Fujimura, N. Togawa, H. Yamamoto, Y. Matsuura, *J. Appl. Phys.* **1984**, *55*, 2083.
[28] J. J. Croat, J. F. Herbst, R. W. Lee, F. E. Pinkerton, *J. Appl. Phys.* **1984**, *55*, 2078.
[29] G. Heatley, P. Sood, D. Goldstein, N. Uriel, J. Cleveland, D. Middlebrook, M. R. Mehra, *J. Heart Lung Transplant.* **2016**, *35*, 528.
[30] H. Yaghoubi, *J. Eng.* **2013**, *2013*, 1.
[31] A. Nemiroski, A. A. Kumar, S. Soh, D. V. Harburg, H. D. Yu, G. M. Whitesides, *Anal. Chem.* **2016**, *88*, 2666.
[32] Q.-H. Gao, G. Yan, H.-X. Zou, W.-M. Zhang, Z.-K. Peng, G. Meng, *IEEE Sens. J.* **2020**, *20*, 1730.
[33] K. A. Mirica, S. S. Shevkoplyas, S. T. Phillips, M. Gupta, G. M. Whitesides, *J. Am. Chem. Soc.* **2009**, *131*, 10049.
[34] S. Ge, G. M. Whitesides, *Anal. Chem.* **2018**, *90*, 12239.
[35] S. Knowlton, A. Joshi, P. Syrrist, A. F. Coskun, S. Tasoglu, *Lab Chip.* **2017**, *17*, 2839.
[36] E. Turker, A. Arslan-Yildiz, *Tissue Eng.* **2018**, *4*, 787.
[37] S. Yaman, H. C. Tekin, *Anal. Chem.* **2020**, *92*, 12556.
[38] M. Baday, S. Calamak, N. G. Durmus, R. W. Davis, L. M. Steinmetz, U. Demirci, *Small* **2016**, *12*, 1222.
[39] O. Sarigil, M. IneviAnil-, E. Yilmaz, G. Mese, H. C. Tekin, E. Ozcivici, *Analyst* **2019**, *144*, 2942.
[40] E. Yilmaz, E. Ozcivici, H. C. Tekin, presented at *2019 Innovations in Intelligent Systems and Applications Conf. (ASYU)*, IEEE Izmir, Turkey **2019**.

© 2021 The Authors. Advanced NanoBiomed Research published by Wiley-VCH GmbH

26999307, 2022, 3, Downloaded from https://advanced.onlinelibrary.wiley.com/doi/10.1002/anbr.202100103 by Koc University, Wiley Online Library on [05/09/2026]. See the Terms and Conditions (https://onlinelibrary.wiley.com/terms-and-conditions) on Wiley Online Library for rules of use; OA articles are governed by the applicable Creative Commons License

[41] S. Knowlton, I. Sencan, Y. Aytar, J. Khoory, M. M. Heeney, I. C. Ghiran, S. Tasoglu, *Sci Rep.* **2015**, *5*, 15022.
[42] S. Tasoglu, J. A. Khoory, H. C. Tekin, C. Thomas, A. E. Karnoub, I. C. Ghiran, U. Demirci, *Adv. Mater.* **2015**, *27*, 3901.
[43] A. A. Ashkarran, M. Mahmoudi, *Phys. Educ.* **2021**, *56*, 055020.
[44] K. A. Mirica, S. T. Phillips, C. R. Mace, G. M. Whitesides, *J. Agric. Food Chem.* **2010**, *58*, 6565.
[45] A. A. Ashkarran, K. S. Suslick, M. Mahmoudi, *Anal. Chem.* **2020**, *92*, 1663.
[46] A. A. Ashkarran, T. Olfatbakhsh, M. Ramezankhani, R. C. Crist, W. H. Berrettini, A. S. Milani, S. Pakpour, M. Mahmoudi, *Adv. Healthcare Mater.* **2020**, *9*, 1901608.
[47] N. D. Shapiro, K. A. Mirica, S. Soh, S. T. Phillips, O. Taran, C. R. Mace, S. S. Shevkoplyas, G. M. Whitesides, *J. Am. Chem. Soc.* **2012**, *134*, 5637.
[48] N. D. Shapiro, S. Soh, K. A. Mirica, G. M. Whitesides, *Anal. Chem.* **2012**, *84*, 6166.
[49] N. Puluca, N. G. Durmus, S. Lee, N. Belbachir, F. X. Galdos, M. G. Ogut, R. Gupta, K. Hirano, M. Krane, R. Lange, J. C. Wu, S. M. Wu, U. Demirci, *Adv. Biosyst.* **2020**, *4*, 1900300.
[50] K. Delikoyun, S. Yaman, E. Yilmaz, O. Sarigil, M. Anil-Inevi, K. Telli, O. Yalcin-Ozuysal, E. Ozcivici, H. C. Tekin *ACS Sens.* **2020**, *6*, 2191.
[51] A. B. Subramaniam, M. Gonidec, N. D. Shapiro, K. M. Kresse, G. M. Whitesides, *Lab Chip* **2015**, *15*, 1009.
[52] S. S. Deshmukh, B. Shakya, A. Chen, A. Chen, N. G. Durmus, B. Greenhouse, E. S. Egan, U. Demirci, *Commun. Biol.* **2021**, *4*, 1.
[53] A. Winkleman, K. L. Gudiksen, D. Ryan, G. M. Whitesides, D. Greenfield, M. Prentiss, *Appl. Phys. Lett.* **2004**, *85*, 2411.
[54] S. Libring, Á. Enríquez, H. Lee, L. Solorio, *Cancers* **2021**, *13*, 4440.
[55] K. Delikoyun, A. A. Demir, H. C. Tekin, presented at *Label-free Biomedical Imaging and Sensing (LBIS)* SPIE BiOS **2021** Online Only.
[56] L. Digiacomo, E. Quagliarini, V. La Vaccara, A. Coppola, R. Coppola, D. Caputo, H. Amenitsch, B. Sartori, G. Caracciolo, D. Pozzi, *Cancers* **2021**, *13*, 5155.
[57] M. S. Andersen, S. Lu, G. J. Lopez, A. T. Lassen, N. I. Shapiro, I. C. Ghiran, *Shock* **2019**, *51*, 147.
[58] F. Ozefe, A. A. Yildiz, *Analyst* **2020**, *145*, 5816.
[59] B. Yenilmez, S. Knowlton, S. Tasoglu, *Adv. Mater. Technol.* **2016**, *1*, 1600144.
[60] M. R. Lockett, K. A. Mirica, C. R. Mace, R. D. Blackledge, G. M. Whitesides, *J. Forensic Sci.* **2013**, *58*, 40.
[61] D. Y. Urey, H. M. Chan, N. G. Durmus, *Adv. Biol.* **2021**, *5*, 2000441.
[62] J. T. Caleffi, M. C. E. Aal, O. M. Gallindo Hde, G. H. Caxali, B. P. Crulhas, A. O. Ribeiro, G. R. Souza, K. Delella Fávia, *Life Sci.* **2021**, *286*, 120028.
[63] M. Anil-Inevi, K. Delikoyun, G. Mese, H. Cumhur Tekin, E. Ozcivici, *Biotechnol. Bioeng.* **2021**, *118*, 4771.
[64] M. Inevi-Anil, S. Yaman, A. A. Yildiz, G. Mese, O. Yalcin-Ozuysal, H. Cumhur Tekin, E. Ozcivici, *Sci. Rep.* **2018**, *8*, 7239.
[65] W. L. Haisler, D. M. Timm, J. A. Gage, H. Tseng, T. Killian, G. R. Souza *Nat. Protoc.* **2013**, *8*, 1940.
[66] O. Sarigil, M. Anil-Inevi, E. Yilmaz, O. Ozcelik, G. Mese, H. Cumhur Tekin, E. Ozcivici, presented at *2020 Medical Technologies Congress (TIPTEKNO)*, IEEE Antalya, Turkey **2020**.
[67] I. Gaitán-Salvatella, E. O. -VillegasLópez, P. González-Alva, F. -OlmosSusate, M. A. Pérez-Álvarez, *Front. Mol. Biosci.* **2021**, *8*, 672518.
[68] *'Magnate' and 'Magnet': Poles Apart*, Merriam-Webster, Incorporated, https://www.merriam-webster.com/words-at-play/magnate-vs-magnet-usage-difference (accessed: June 2021).
[69] I. Baker, I. Baker, *Fifty Materials that Make the World*, Springer, Switzerland AG **2018**, pp. 187–194.
[70] D. Jiles *Introduction to Magnetism and Magnetic Materials*, CRC press, Boca Raton, FL **2015**.
[71] M. E. Cano, T. FragaCordova-, M. Sosa, J. Bernal-Alvarado, O. Baffa, *Eur. J. Phys.* **2008**, *29*, 345.
[72] N. A. Spaldin, *Magn. Mater.* **2010**, *9780521886697*, 3.
[73] A. S. Wahajuddin, *Int. J. Nanomed.* **2012**, *7*, 3445.
[74] M. R. Liebowitz, *J. Clin. Psychiatry* **1993**, *54*, 10.
[75] N. Pamme, *Lab Chip* **2006**, *6*, 24.
[76] F. Armstrong, W. Teo, *Anaesth. Intensive Care Med.* **2020**, *21*, 252.
[77] S. Huang, Y. Q. He, F. Jiao, *Chin. J. Anal. Chem.* **2017**, *45*, 1238.
[78] Q. Cao, Q. Fan, Q. Chen, C. Liu, X. Han, L. Li, *Mater. Horiz.* **2020**, *7*, 638.
[79] N. Modak, A. Datta, R. Ganguly, *Microfluid. Nanofluid.* **2008**, *6*, 647.
[80] A. H. Ng, K. Choi, R. P. Luoma, J. M. Robinson, A. R. Wheeler, *Anal Chem.* **2012**, *84*, 8805.
[81] R. Zhou, C. Wang, *Microfluid. Nanofluid.* **2016**, *20*, 1.
[82] Nasiri R., Shamloo A., Ahadian S., L. Amirifar, J. Akbari, M. J. Goudie, K. Lee, N. Ashammakhi, M. R. Dokmeci, D. Di Carlo, A. Khademhosseini, *Small* **2020**, *16*, 2000171.
[83] Y. Wang, Y. Zhao, S. K. Cho, *J. Micromech. Microeng.* **2007**, *17*, 2148.
[84] D. Lombardi, P. S. Dittrich, *Anal. Bioanal. Chem.* **2011**, *399*, 347.
[85] Y. Zhang, N. T. Nguyen, *Lab Chip* **2017**, *17*, 994.
[86] E. Mirowski, J. Moreland, A. Zhang, S. E. Russek, M. J. Donahue, *Appl. Phys. Lett.* **2005**, *86*, 1.
[87] D. Matsunaga, F. Meng, A. Zottl, R. Golestanian, J. M. Yeomans, *Phys. Rev. Lett.* **2017**, *119*, 198002.
[88] J. Yang, J. Gunn, S. R. Dave, M. Zhang, Y. A. Wang, X. Gao, *Analyst* **2008**, *133*, 154.
[89] M. Zborowski, J. J. Chalmers, In *Wiley Encyclopedia of Electrical and Electronics Engineering*, (Ed: J.G. Webster), New York City, United States **2015**, p. 1.
[90] N.-T. Nguyen, Z. Wu, *J. Micromech. Microeng.* **2005**, *15*, R1.
[91] G. P. Zhu, N. T. Nguyen, *Lab Chip.* **2012**, *12*, 4772.
[92] M. Saadat, M. B. Shafii, M. Ghassemi, *Chem. Eng. Process.* **2020**, *147*, 107727.
[93] M. Saadat, M. Ghassemi, M. B. Shafii, *Energy Sources, Part A* **2020**, 1.
[94] W. Zhao, R. Cheng, J. R. Miller, L. Mao, *Adv. Funct. Mater.* **2016**, *26*, 3916.
[95] C. Zhang, P. Zhao, W. Wen, J. Xie, N. Xia, J. Fu, *Polym. Test.* **2018**, *70*, 520.
[96] C. Zhang, P. Zhao, D. Tang, N. Xia, X. Zhang, J. Nie, F. Gu, H. Zhou, J. Fu, *Sens. Actuators, B: Chem.* **2020**, *304*, 127362.
[97] Q. Cao, A. Ding, J. Liu, X. Han, *IEEE Sens. J.* **2020**, *20*, 14065.
[98] C. Zhang, P. Zhao, F. Gu, X. Zhang, J. Xie, Y. He, H. Zhou, J. Fu, L.-S. Turng, *Anal. Chem.* **2020**, *92*, 6925.
[99] C. Zhang, P. Zhao, F. Gu, J. Xie, N. Xia, Y. He, J. Fu, *Anal. Chem.* **2018**, *90*, 9226.
[100] S. Ge, Y. Wang, N. J. Deshler, D. J. Preston, G. M. Whitesides, *J. Am. Chem. Soc.* **2018**, *140*, 7510.
[101] A. Nemiroski, S. Soh, S. W. Kwok, H. D. Yu, G. M. Whitesides, *J. Am. Chem. Soc.* **2016**, *138*, 1252.
[102] J. Xie, P. Zhao, C. Zhang, Y. Hao, N. Xia, J. Fu, *Measurement* **2019**, *136*, 564.
[103] Q.-H. Gao, W.-M. Zhang, H.-X. Zou, F.-R. Liu, W.-B. Li, Z.-K. Peng, G. Meng, *Appl. Phys. Lett.* **2018**, *112*, 142408.
[104] R. Amin, S. Knowlton, B. Yenilmez, A. Hart, A. Joshi, S. Tasoglu *RSC Adv.* **2016**, *6* 93922.
[105] A. A. Ashkarran, N. Dararatana, D. Crespy, G. Caracciolo, M. Mahmoudi, *Nanoscale.* **2020**, *12*, 2374.
[106] N. G. Durmus, H. C. Tekin, S. Guven, K. Sridhar, A. A. Yildiz, G. Calibasi, I. Ghiran, R. W. Davis, L. M. Steinmetz, U. Demirci, *Proc. Natl. Acad. Sci.* **2015**, *112*, E3661.

© 2021 The Authors. Advanced NanoBiomed Research published by Wiley-VCH GmbH

26999307, 2022, 3, Downloaded from https://advanced.onlinelibrary.wiley.com/doi/10.1002/anbr.202100103 by Koc University, Wiley Online Library on [05/09/2026]. See the Terms and Conditions (https://onlinelibrary.wiley.com/terms-and-conditions) on Wiley Online Library for rules of use; OA articles are governed by the applicable Creative Commons License

[107] O. Sarigil, M. Anil-Inevi, E. Yilmaz, M. Cagan, G. Mese, H. Cumhur Tekin, E. Ozcivici, presented at IEEE Istanbul, Turkey *2019 9th Int. Conf. on Recent Advances in Space Technologies (RAST)*, **2019**.
[108] M. S. Andersen, E. Howard, S. Lu, M. Richard, M. Gregory, G. Ogembo, O. Mazor, P. Gorelik, N. I. Shapiro, A. V. Sharda, I. Ghiran, *Lab Chip* **2017**, *17*, 3462.
[109] E. J. Felton, A. Velasquez, S. Lu, R. O. Murphy, A. ElKhal, O. Mazor, P. Gorelik, A. Sharda, I. C. Ghiran, *Lab Chip* **2016**, *16*, 3286.
[110] M. Baday, O. Ercal, A. Z. Sahan, A. Sahan, B. Ercal, H. Inan, U. Demirci, *Adv. Healthcare Mater.* **2019**, *8*, 1801517.
[111] R. Amin, S. Knowlton, J. Dupont, J. S. Bergholz, A. Joshi, A. Hart, B. Yenilmez, C. H. Yu, A. Wentworth, J. J. Zhao, S. Tasoglu, *J. 3D Print. Med.* **2017**, *1*, 155.
[112] R. Amin, S. Knowlton, A. Hart, B. Yenilmez, F. Ghaderinezhad, S. Katebifar, M. Messina, A. Khademhosseini, S. Tasoglu, *Biofabrication* **2016**, *8*, 022001.
[113] S. R. Dabbagh, M. R. Sarabi, R. Rahbarghazi, E. Sokullu, A. K. Yetisen, S. Tasoglu, *iScience.* **2020**, *24*, 102012.
[114] C. Hepatitis, *World Health Organization (WHO)*, **2020**, https://www.who.int/news-room/fact-sheets/detail/hepatitis-c (accessed :June 2021).
[115] B. Yenilmez, S. Knowlton, C. H. Yu, M. M. Heeney, S. Tasoglu, *Adv. Mater. Technol.* **2016**, *1*, 1600100.
[116] M. Ravi, V. Paramesh, S. Kaviya, E. Anuradha, F. P. Solomon, *J. Cell. Physiol.* **2015**, *230*, 16.
[117] S. Knowlton, Y. Cho, X.-J. Li, A. Khademhosseini, S. Tasoglu, *Biomater. Sci.* **2016**, *4*, 768.
[118] E. Lepowsky, M. Muradoglu, S. Tasoglu, *Bioprinting.* **2018**, *11*, 00034.
[119] R. Tiruvannamalai-Annamalai, D. R. Armant, H. W. Matthew, *PLoS One* **2014**, *9*, e84287.
[120] A. Ovsianikov, A. Khademhosseini, V. Mironov, *Trends Biotechnol.* **2018**, *36*, 348.
[121] Z. Dai, J. Ronholm, Y. Tian, B. Sethi, X. Cao, *J. Tissue Eng.* **2016**, *7*, 204173141664881.
[122] F. N. Alaribe, S. L. Manoto, S. C. K. M. Motaung, *Biologia* **2016**, *71*, 353.
[123] Ž. P. Kačarević, P. M. Rider, S. Alkildani, S. Retnasingh, R. Smeets, O. Jung, Z. Ivanišević, M. Barbeck, *Materials.* **2018**, *11*, 2199.
[124] N. Hong, G. H. Yang, J. Lee, G. Kim, *J. Biomed. Mater. Res. Part B* **2018**, *106*, 444.
[125] J. Y. Park, J. Jang, H.-W. Kang, *Microelectron Eng.* **2018**, *200*, 1.
[126] M. Ustun, S. Dabbagh Rahmani, I. S. Ilci, T. Bagci-Onder, S. Tasoglu, *Micromachines* **2021**, *12*, 490.
[127] S. Chameettachal, S. Yeleswarapu, S. Sasikumar, P. Shukla, P. Hibare, A. K. Bera, S. S. R. Bojedla, F. Pati, *J. Indian Inst. Sci.* **2019**, *99*, 375.
[128] K. A. Mirica, F. Ilievski, A. K. Ellerbee, S. S. Shevkoplyas, G. M. Whitesides, *Adv. Mater.* **2011**, *23*, 4134.
[129] A. C. Daquinag, G. R. Souza, M. G. Kolonin, *Tissue Eng. Part C: Methods* **2013**, *19*, 336.
[130] E. Türker, N. Demirçak, A. Arslan-Yildiz, *Biomater. Sci.* **2018**, *6*, 1745.
[131] R. Onbas, A. Yildiz Arslan, *ACS Appl. Bio Mater.* **2021**, *4*, 1794.
[132] H. Jaganathan, J. Gage, F. Leonard, S. Srinivasan, G. R. Souza, B. Dave, B. Godin, *Sci. Rep.* **2014**, *4*, 1.
[133] H. Tseng, L. R. Balaoing, B. Grigoryan, R. M. Raphael, T. C. Killian, G. R. Souza, K. J. Grande-Allen, *Acta Biomater.* **2014**, *10*, 173.
[134] A. A. Ashkarran, M. Mahmoudi, *Trends Biotechnol.* **2020**, *39*, 311.
[135] D. K. Bwambok, M. M. Thuo, M. B. Atkinson, K. A. Mirica, N. D. Shapiro, G. M. Whitesides, *Anal. Chem.* **2013**, *85*, 8442.
[136] S. Knowlton, A. Joshi, B. Yenilmez, I. T. Ozbolat, C. K. Chua, A. Khademhosseini, S. Tasoglu, *Int. J. Bioprinting* **2013**, *85*, 17, 8442.
[137] Z. Luo, S. Güven, I. Gozen, P. Chen, S. Tasoglu, R. M. Anchan, B. Bai, U. Demirci, *Microfluid. Nanofluid.* **2015**, *19*, 883.
[138] B. Ozdalgic, M. Ustun, S. R. Dabbagh, B. Z. Haznedaroglu, A. Kiraz, S. Tasoglu, *Biotechnol. Bioeng.* **2021**, *118*, 1716.
[139] R. Amin, F. Ghaderinezhad, L. Li, E. Lepowsky, B. Yenilmez, S. Knowlton, S. Tasoglu, *Anal. Chem.* **2017**, *89*, 6351.
[140] M. R. Sarabi, A. Ahmadpour, A. K. Yetisen, S. Tasoglu, *Appl. Sci.* **2021**, *11*, 5329.
[141] M. Temirel, S. R. Dabbagh, S. Tasoglu, *Micromachines* **2021**, *12*, 182.
[142] M. R. Sarabi, N. Jiang, E. Ozturk, A. K. Yetisen, S. Tasoglu, *Lab Chip* **2021**, *21*, 627.
[143] F. Ghaderinezhad, H. C. Koydemir, D. Tseng, D. Karinca, K. Liang, A. Ozcan, S. Tasoglu, *Sci. Rep.* **2020**, *10*, 1.
[144] E. Lepowsky, F. Ghaderinezhad, S. Knowlton, S. Tasoglu, *Biomicrofluidics* **2017**, *11*, 051501.
[145] M. Temirel, B. Yenilmez, S. Tasoglu, *Sci. Rep.* **2021**, *11*, 1.
[146] F. Ozefe, A. A. Yildiz, *Magnetic Levitation*, IntechOpen, London **2020**.
[147] S. R. Dabbagh, F. Rabbi, Z. Doğan, A. K. Yetisen, S. Tasoglu, *Biomicrofluidics* **2020**, *14*, 061506.
[148] J. Riordon, D. Sovilj, S. Sanner, D. Sinton, E. W. Young, *Trends Biotechnol.* **2019**, *37*, 310.
[149] J. Riordon, D. Sovilj, S. Sanner, D. Sinton, E. W. Young, *J. Biol. Phys.* **2021**, 1.
[150] F. Ilievski, K. A. Mirica, A. K. Ellerbee, G. M. Whitesides, *Soft Matter.* **2011**, *7*, 9113.



Sajjad Rahmani Dabbagh is currently a Ph.D. student at Koç University with the focus being on the integration of machine learning and 3D bioprinting for parametric optimization of bioprinting process and defect prediction. His research interests include lab-on-a-chip technologies, point-of-the-care diagnosis, complex fluid mechanics, 3D bioprinting, and artificial intelligence. He graduated from Tabriz University with a bachelor's degree in mechanical engineering in 2016.

© 2021 The Authors. Advanced NanoBiomed Research published by Wiley-VCH GmbH

26999307, 2022, 3, Downloaded from https://advanced.onlinelibrary.wiley.com/doi/10.1002/anbr.202100103 by Koc University, Wiley Online Library on [05/09/2026]. See the Terms and Conditions (https://onlinelibrary.wiley.com/terms-and-conditions) on Wiley Online Library for rules of use; OA articles are governed by the applicable Creative Commons License



Metin Sitti received his B.Sc. and M.Sc. degrees in electrical and electronics engineering from Bogazici University, Turkey, in 1992 and 1994, respectively, and his Ph.D. degree in electrical engineering from the University of Tokyo, Japan, in 1999. He was a research scientist at the University of California at Berkeley during 1999–2002 and a professor at Carnegie Mellon University, USA, during 2002–2014. He is currently a director of the Physical Intelligence Department at the Max-Planck Institute for Intelligent Systems, Stuttgart, Germany and a professor at ETH Zurich, Switzerland and Koc University, Turkey. His research interests include small-scale physical intelligence, mobile milli- and microrobots, soft materials and robots, bioinspired materials, and medical miniature robots.



Savas Tasoglu received his Ph.D. degree in 2011 from UC Berkeley and held a postdoctoral appointment at Harvard Medical School. His research interests are at the interfaces of complex microfluidics, transport phenomena, and biomaterials with applications in biomedicine and biotechnology. He has received several awards, including a Marie Curie Fellowship, American Heart Association Scientist Development Award, NIH K99/R00 Pathway to Independence Award (declined), Alexander von Humboldt Fellowship for Experienced Researchers, and the Wolff New Venture Competition Award.

© 2021 The Authors. Advanced NanoBiomed Research published by Wiley-VCH GmbH

26999307, 2022, 3, Downloaded from https://advanced.onlinelibrary.wiley.com/doi/10.1002/anbr.202100103 by Koc University, Wiley Online Library on [05/09/2026]. See the Terms and Conditions (https://onlinelibrary.wiley.com/terms-and-conditions) on Wiley Online Library for rules of use; OA articles are governed by the applicable Creative Commons License